AD-A105 169 NEW MEXICO UNIV ALBUQUERQUE BUREAU OF ENGINEERING R--ETC F/G 20/9
PHYSICS OF HIGH TEMPERATURE, DENSE PLASMAS.(U)
MAR 81 D M WOODALL AFOSR-79-0060
UNCLASSIFIED NE-91(81)AFOSR-765-2 AFOSR-TR-81-0687 NL

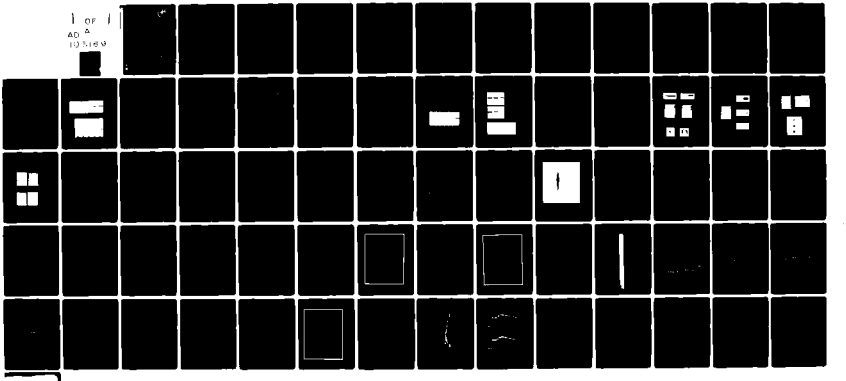

END
DATE FILMED
10-81
DTIC

AFOSR-TR- 81 -0687

LEVEL II

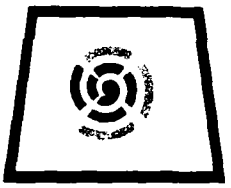

THE UNIVERSITY OF NEW MEXICO
COLLEGE OF ENGINEERING

BUREAU OF ENGINEERING RESEARCH

PHYSICS OF HIGH TEMPERATURE, DENSE PLASMAS

Interim Report

By

D. M. Woodall

Report No. NE-91(81)AFOSR-765-2
Work Performed Under AFOSR [redacted] 79-0060

SECURITY CLASSIFICATION OF THIS PAGE (When Data Entered)

REPORT DOCUMENTATION PAGE

READ INSTRUCTIONS BEFORE COMPLETING FORM

1. REPORT NUMBER (14) (18) AFOSR-TR-81-0687	2. GOVT ACCESSION NO. AD-A105 769
3. RECIPIENT'S CATALOG NUMBER	
4. TITLE (and Subtitle) (6) PHYSICS OF HIGH TEMPERATURE, DENSE PLASMAS	5. TYPE OF REPORT & PERIOD COVERED (9) Interim rept. 01 Jan 80 - 31 Mar 81
6. PERFORMING ORG. REPORT NUMBER (14) NE-91(81)AFOSR-765-2	
7. AUTHOR(s) (10) D. M. Woodall (15)	8. CONTRACT OR GRANT NUMBER(s) AFOSR-79-0060
9. PERFORMING ORGANIZATION NAME AND ADDRESS University of New Mexico College of Engineering Albuquerque, NM 87131	10. PROGRAM ELEMENT, PROJECT, TASK AREA & WORK UNIT NUMBERS (16) 2301/A7 61102F (17) A7
11. CONTROLLING OFFICE NAME AND ADDRESS AFOSR/NP Bolling AFB, Bldg. #410 Washington, DC 20332 (12) 66	12. REPORT DATE Mar. 1981 (11) Mar. 13. NUMBER OF PAGES 61 81
14. MONITORING AGENCY NAME & ADDRESS (if different from Controlling Office)	15. SECURITY CLASS. (of this report) Unclassified
	15a. DECLASSIFICATION DOWNGRADING SCHEDULE

16. DISTRIBUTION STATEMENT (of this Report)

Approved for public release; distribution unlimited

17. DISTRIBUTION STATEMENT (of the abstract entered in Block 20, if different from Report)

18. SUPPLEMENTARY NOTES

19. KEY WORDS (Continue on reverse side if necessary and identify by block number)

20. ABSTRACT (Continue on reverse side if necessary and identify by block number)

This interim report details activities under AFOSR Grant 79-0060 during the period of Jan 1980-March 81. The grant, "The Physics of High Temperature, Dense Plasmas," includes work on two projects in conjunction with the Advanced Concepts Branch of the Applied Physics Division at the Air Force Weapons Laboratory. The first is a relativistic electron beam-(REB) heated, dense plasma experiment using REB facilities at AFWL, and the second is soft x-ray instrumentation work pertinent to the SHIVA x-ray simulation facility. This —>cont

DD FORM 1 JAN 73 1473 EDITION OF 1 NOV 65 IS OBSOLETE

Unclassified 256085

SECURITY CLASSIFICATION OF THIS PAGE (When Data Entered)

report primarily details work in progress and results achieved in the REB-Plasma interaction experiments, since much of our effort during the period of this report have been directed at that project.

Accession For	
NTIS GRA&I	☒
DTIC TAB	☐
Unannounced	☐
Justification	
By	
Distribution/	
Availability Codes	
Dist	Avail and/or Special
A	

BLANK PAGE

"Physics of High Temperature, Dense Plasmas"

D. M. Woodall, Principal Investigator

University of New Mexico

Interim Report

Period: Jan. 1980-Mar.1981

AFOSR Grant - 79-0060

BLANK PAGE

TABLE OF CONTENTS

I. Introduction

This interim report details activities under AFOSR Grant 79-0060 during the period of Jan 1980-March 1981. That grant, "The Physics of High Temperature, Dense Plasmas." includes work on two projects in conjunction with the Advanced Concepts Branch of the Applied Physics Division at the Air Force Weapons Laboratory (AFWL). The first is a relativistic electron beam-(REB) heated, dense plasma experiment using REB facilities at AFWL, and the second is soft x-ray instrumentation work pertinent to the SHIVA x-ray simulation facility. This report primarily details work in progress and results achieved in the REB-Plasma interaction experiments, since much of our effort during the period of this report have been directed at that project.

II. Development and Characterization of Dense Plasma Source for REB-Plasma Heating Experiments

There has developed recently considerable interest in the anomalous heating of a dense plasma by a relativistic electron beam [1-3]. Low power experiments [4] have indicated that the relativistic two-stream instability can cause a significant enhancement over the energy deposition expected classically. Calculations indicate that scaling to currently available power supplies would allow a plasma of 10^{18}-10^{20}/cm^3 density to be heated to 30-50 kev. Our goal has been to produce a fully-ionized hydrogen plasma with a density of 2×10^{18}/cm^3 and a temperature of 5-10 eV with small spatial gradients. That plasma is to be used in a REB-plasma heating experiment with the low divergence, annular beam from the PR1590 [5]. The work reported here is in the operation and characterization of the plasma source for such an experiment [planned for the final year of our grant].

A. Results to Date

Our experiments take place in the Plasma Physics Laboratory at the Electron Beam facilities at the Air Force Weapons Laboratory. The plasma source used in the experiments is a co-axial plasma gun [6,7] which is capable of operating either in prefilled mode or puffed mode. In the prefilled mode, the plasma gun chamber is operated with a backfill of the desired gas at a selected pressure. In this case the gun operates in the "snowplow" mode whereby the plasma sheath sweeps up the neutral gas in front of it and subsequently ionizes it.

In the puffed mode the chamber is evacuated to below 1 mtorr, and the gun discharge is initiated by the puffing of gas into the back of the gun by an electromagnetic puff valve. The puff valve is backed by a gas plenum pressurized to 20 psi of gas and is operated with a capacitive discharge through a coil. When a capacitor (40 μF) changed to 1-5 kV is allowed to discharge through the coil, it opens up the valve for a short period (on

the order of a msec) and the puff of gas that enters is capable of filling the gun up to a few torr of pressure. In the puffed mode, the gun operation is mainly via the deflagration process with the gas discharge staying near the insulator. The various components of the gun are shown in Figure II.1.

Figure II.2 shows a diagram of the experimental set-up. The main capacitor bank is comprised of six 40 μF (10 kV) capacitors connected in parallel. It is switched by using a krytron trigger circuit and an ignitron switch. A crowbar circuit is incorporated to avoid unwanted LC ringing. The quartz windows of the vacuum chamber are used for optical diagnostic access. The plasma was fired in both operating modes into a longitudinal magnetic field. Since the REB-plasma heating experiments are to take place in 50-100 kG fields, it is necessary to inject the plasma into such a field. The external magnet around the drift-tube is capable of producing a field in excess of 50 kG. It is driven by a set of twelve 180 μF (8 kV) capacitors. Timing of the firing sequence is accomplished by a Maxwell trigger-delay generator unit. All measurements and signals are recorded on Tektronix 7000 series oscilloscopes.

The main objective of our experiment is to produce a high-density, fully-ionized plasma target for a relativistic electron beam (REB) heating experiment. The desired plasma parameters are $n > 10^{18}$ cm^{-3} at a few electron volts with small spatial gradients. Since our REB machine (Pulserad 1590) produces a cold annular beam, an annular plasma target is preferred.

In this paper, we will report on studies of the longitudinal injection of the plasma into a magnetic field and on the various diagnostics for the measurement of the plasma density and temperature. Our diagnostics include visible light spectroscopy (Stark-broadening of H_β line), B-dot probe measurements, Rogowski current monitors, bank voltage measurements, and streak and framing photography. Laser interferometer is currently being set up and electric probes are planned for the near future.

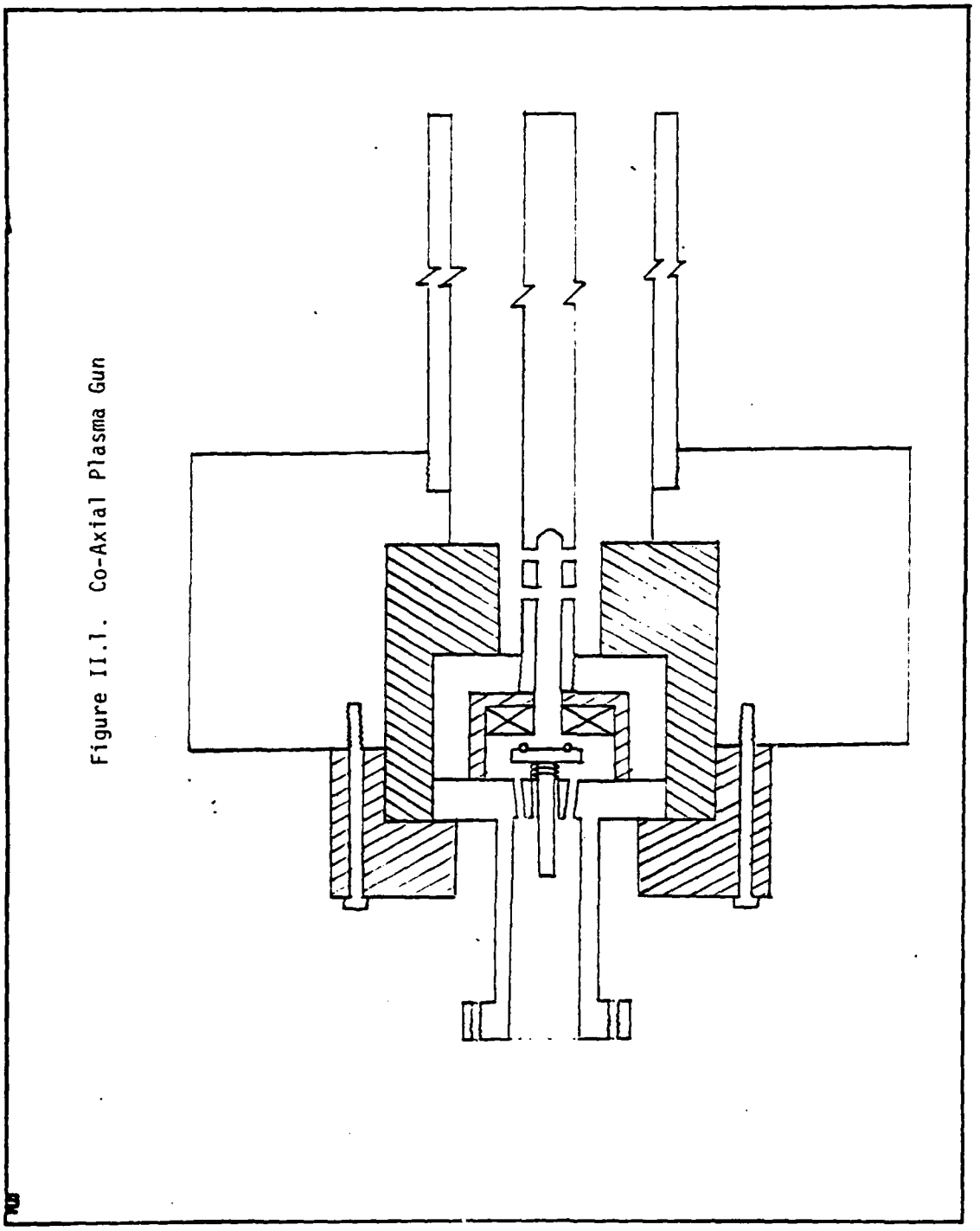

Figure II.1. Co-Axial Plasma Gun

Figure II.2. Experimental Arrangement

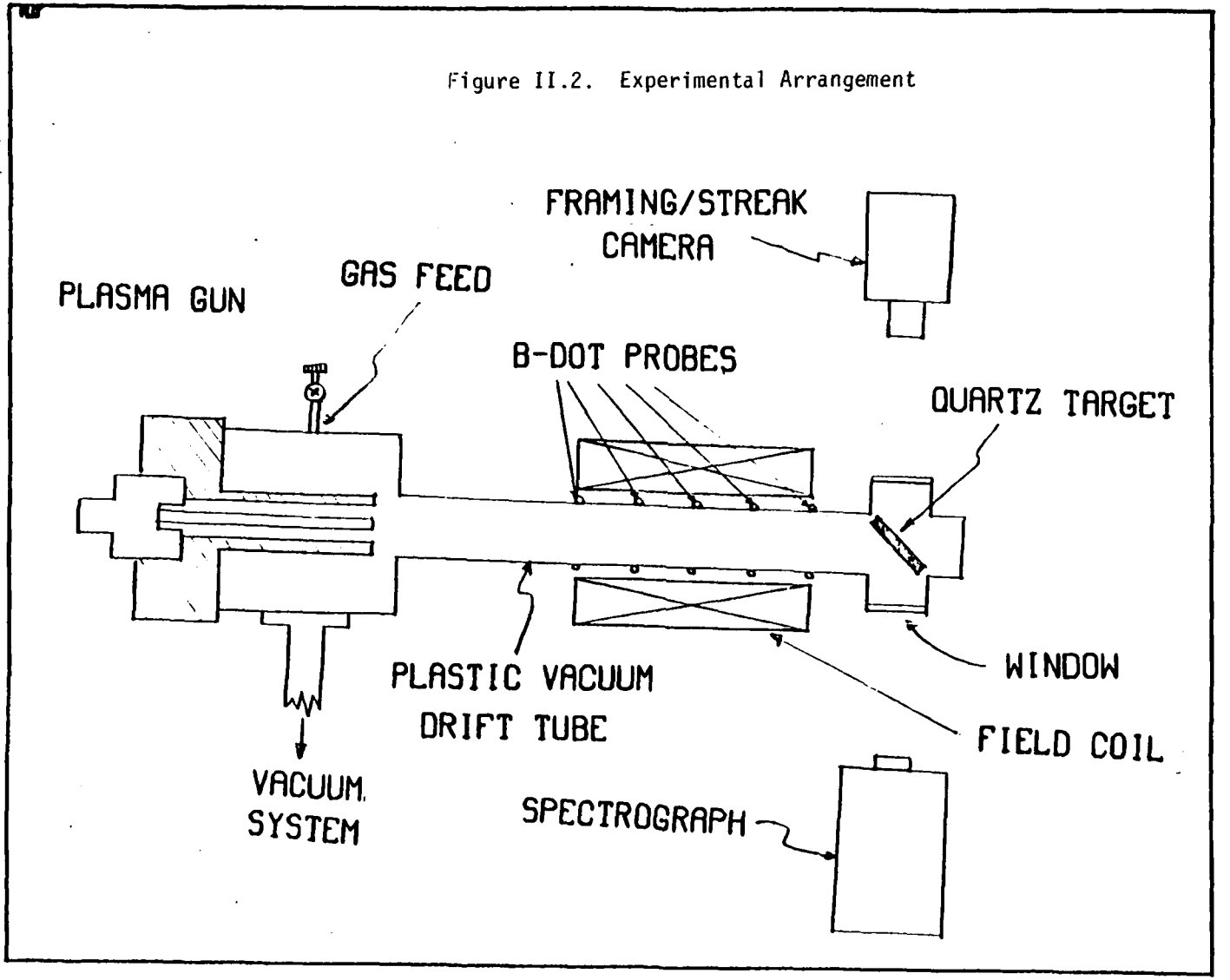

1. Stark Broadening Measurement of the Hβ Line of Hydrogen

A half-meter visible spectrograph (Jarrell Ash Ebert scanning spectrometer, Model 82-000) was used to obtain a time-integrated spectrum of the plasma. The spectra were recorded on polaroid type 57 film (ASA 3000), and were then analyzed using an analysis scheme developed by Dr. M. Collins Clark of AFWL. The program running on a PDP 11/60 digitizes the spectra (with the use of a (Colorado Video) vidicon camera and an image digitizer). The output is in two forms, namely, a 2-D array of intensities, and a plot of the special intensity along an energy scan. In order to minimize measurement errors (primarily electronic noise in the vidicon system), the computer averages data over 1000 line-scans. Measurements were made for both the prefilled and the puffed modes of operation. These measurements were done with no external magnetic field. The drift tube in this experiment was stainless steel and the insulator used in the gun was quartz. Subsequent experiments were performed with quartz and plastic drift tubes to observe the spatial variation of plasma visible light emission.

a. Prefilled Mode.

The spectra for different prefilled pressures at 7 kV bank voltage are shown in Figure II.3. It can be seen that the plasma is quite clean, with only a small amount of Cu and Al lines which originated from the electrodes of the gun. Those lines probably appear late in time, after the discharge is over. Figures II.4 (a), (b), and (c) show some spectra plotted by the PDP 11/60. As the density of the plasma increases, there is a corresponding increase of the H_β linewidth. The densities calculated are listed in Table 1. Since the energy supplied remains constant (9 kV charge) as the prefilled pressure is being increased, the percentage of ionization drops (last column in Table 1).

Figure II.3. Prefill Operation

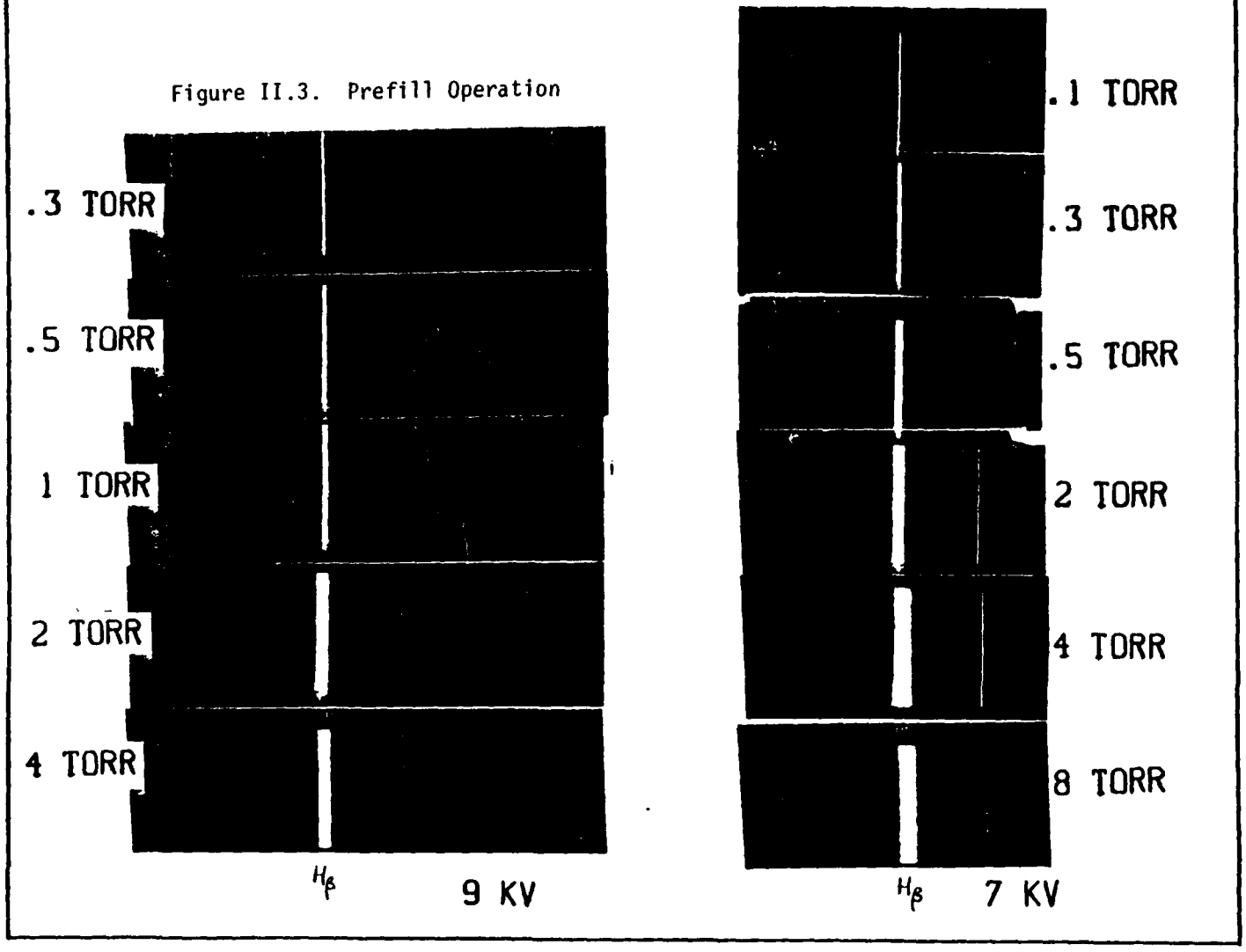

Figure II.4(a). 4 Torr (Prefilled); 9KV Charge at Gun; 50 Micro Slit at 5000A

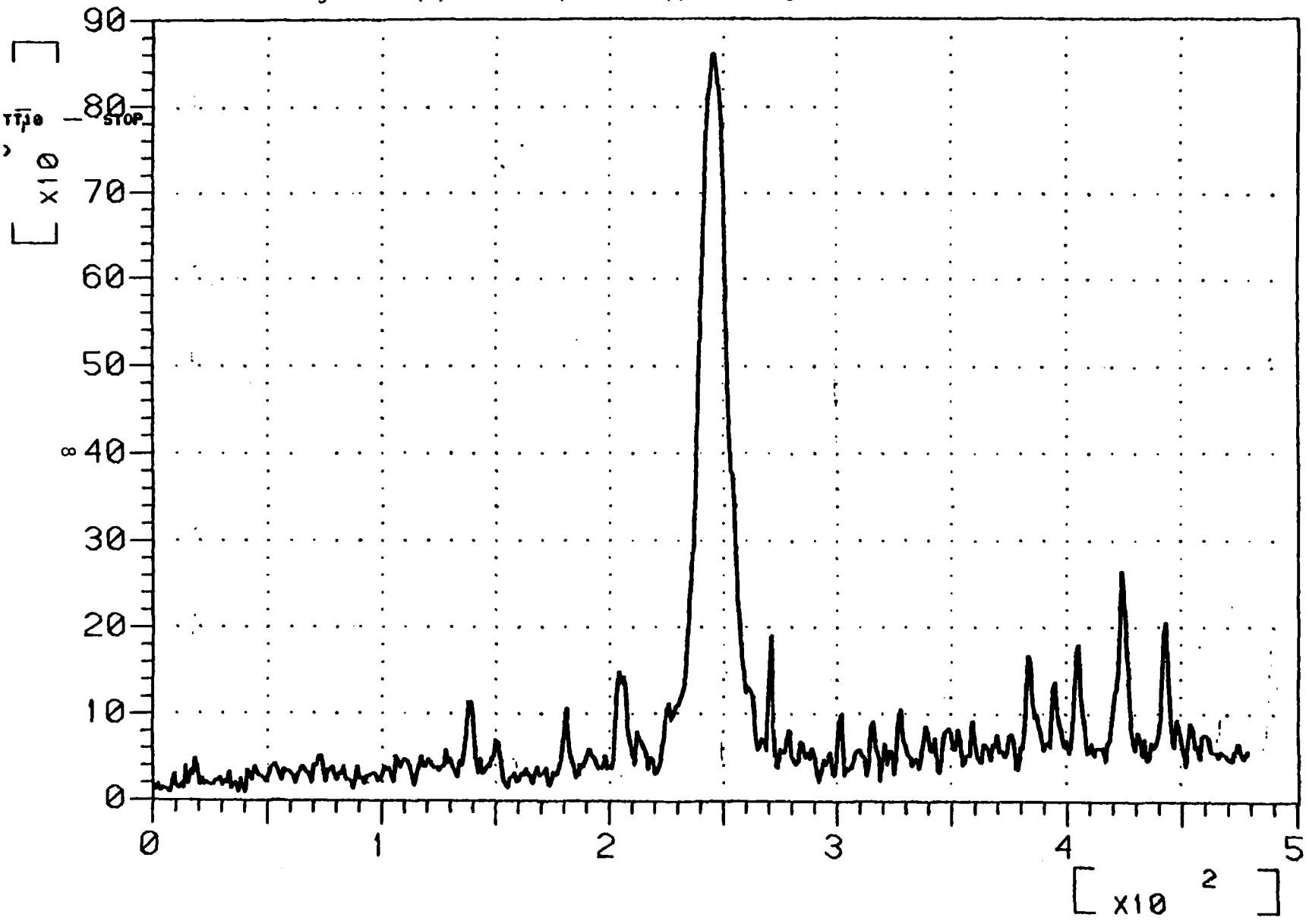

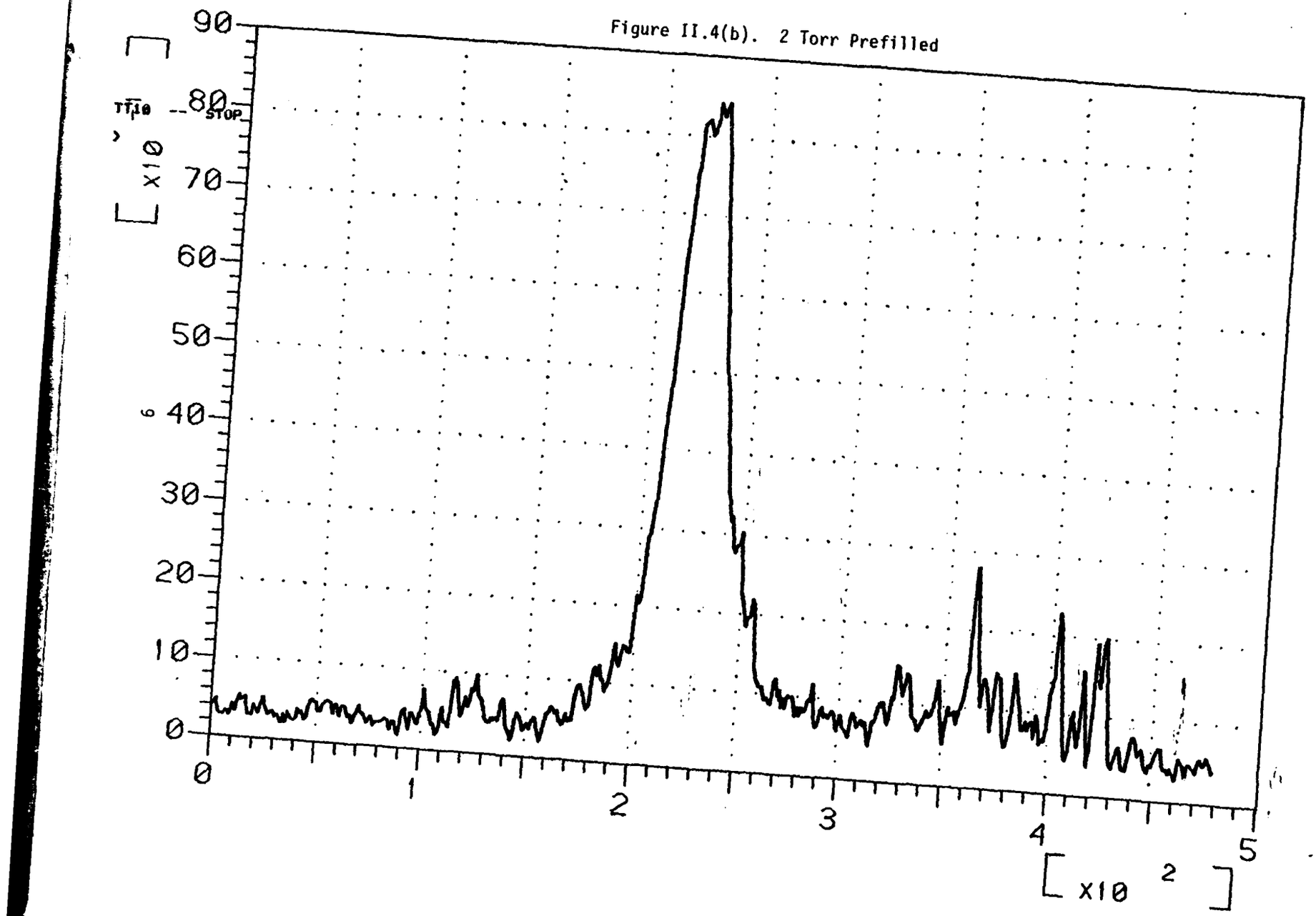
Figure II.4(b). 2 Torr Prefilled
TIME --STOP
X10
90
80
70
60
50
40
30
20
10
0
0
1
2
3
4
5
X10 2

Figure II.4(c). 4 Torr (Prefilled)

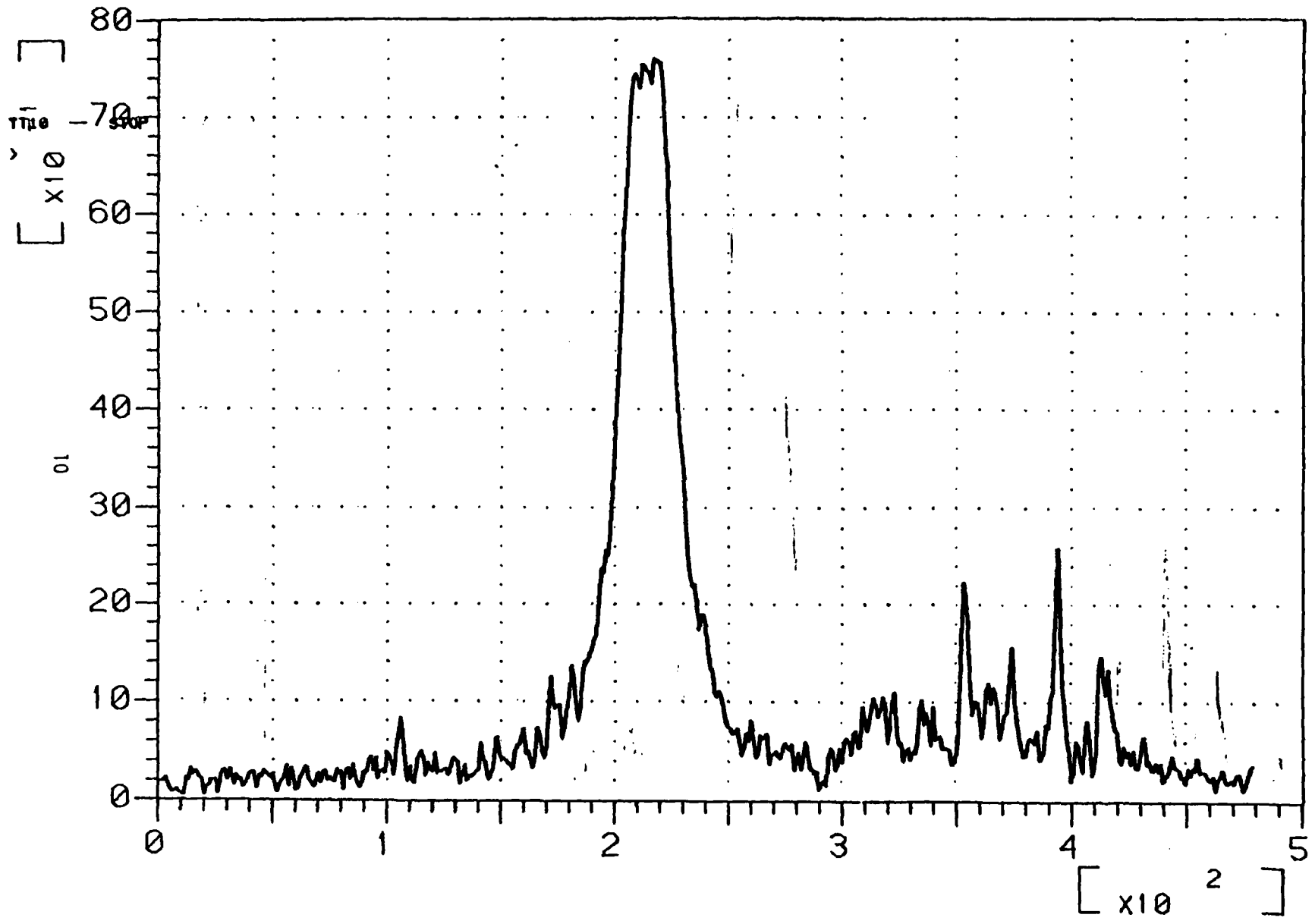

Table 1

Measured Versus Computed Plasma Density
as a Function of Prefill Gas Pressures

Pressure (torr)	Measured Plasma Density (cm^{-3})	Computed Gas Number Density (cm^{-3})	Percentage of Ionization
0.1	6.0×10^{15}	6.0×10^{15}	100
0.3	1.8×10^{16}	1.8×10^{16}	100
0.5	3.0×10^{16}	3.0×10^{16}	100
1.0	5.6×10^{16}	6.0×10^{16}	93
2.0	7.6×10^{16}	1.2×10^{17}	57.5
4.0	1.3×10^{17}	2.4×10^{17}	50
8.0	1.3×10^{17}	4.7×10^{17}	23

Note: Plasma gun being operated at 7 kV.

b. Puffed mode.

In this mode of operation, the puff valve (which is backed by a hydrogen gas plenum at 20 psi) is first fired, then at a pre-selected time the gun bank is fired. With the puff-valve capacitor charged to 1 kV, the final pressure in the gun chamber is around 2 torr. Figure II.5 shows the spectra obtained at different delay times (the gun being fired at 7 kV). Densities calculated are shown in the graph in Figure II.5. Note the transition which occurs in the data with delay time. The early time firing corresponds to the deflagration case, while the late time corresponds to the pre-fill case (since the gas fills the gun cylinder prior to gun discharge).

2. Injection into an External Magnetic Field

Plasma injection into an external magnetic field of up to 30 kG was examined in the prefilled mode. The stainless steel drift tube was replaced by a plastic (Lexan) one to enable measurement of the B-dot signal corresponding to plasma arrival. The original quartz insulator in the gun was replaced by a polycarbonate (Lexan) insulator, due to delay in acquiring quartz replacements. Visible line spectra obtained are shown in Figure II.6. It can be seen that the Lexan insulator has introduced copious amounts of impurities into the plasma. As the magnetic field increases, the H_β linewidth decreases, indicating that the plasma which penetrates the field has lower density. It can also be seen that at high voltages, the linewidths are larger. Thus a more energetic plasma penetrates more easily into the B-field, as expected. For further work we have gone to a 20 Kv gun which can operate at higher densities and higher total energies.

3. Framing and Streak Photography

Some framing and streak photographs were taken with a TRW image-converter camera. A quartz target was introduced into the

Figure II.5. Puffed Operation

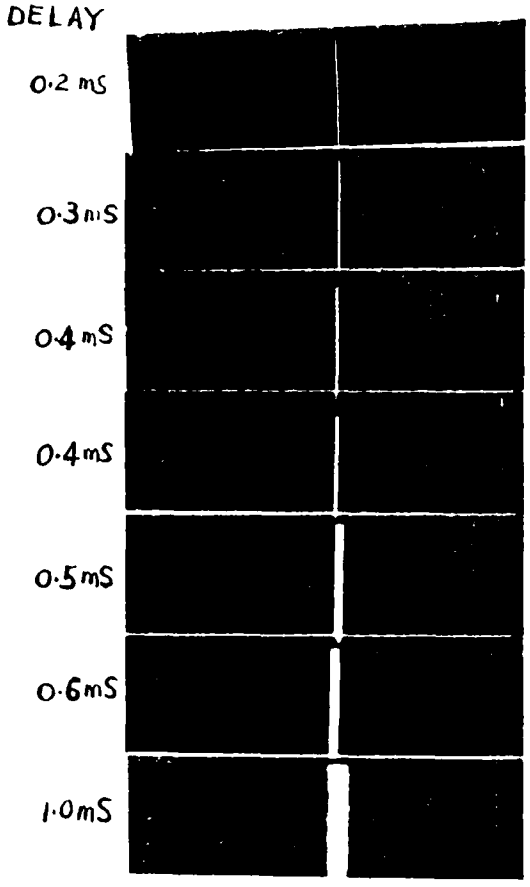

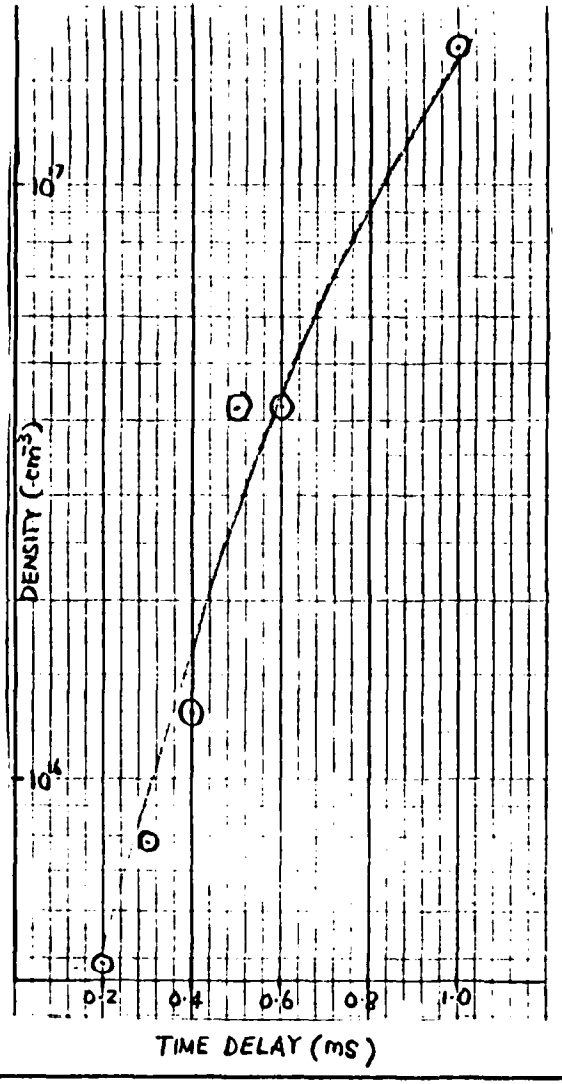

Figure II.6. Prefill Data

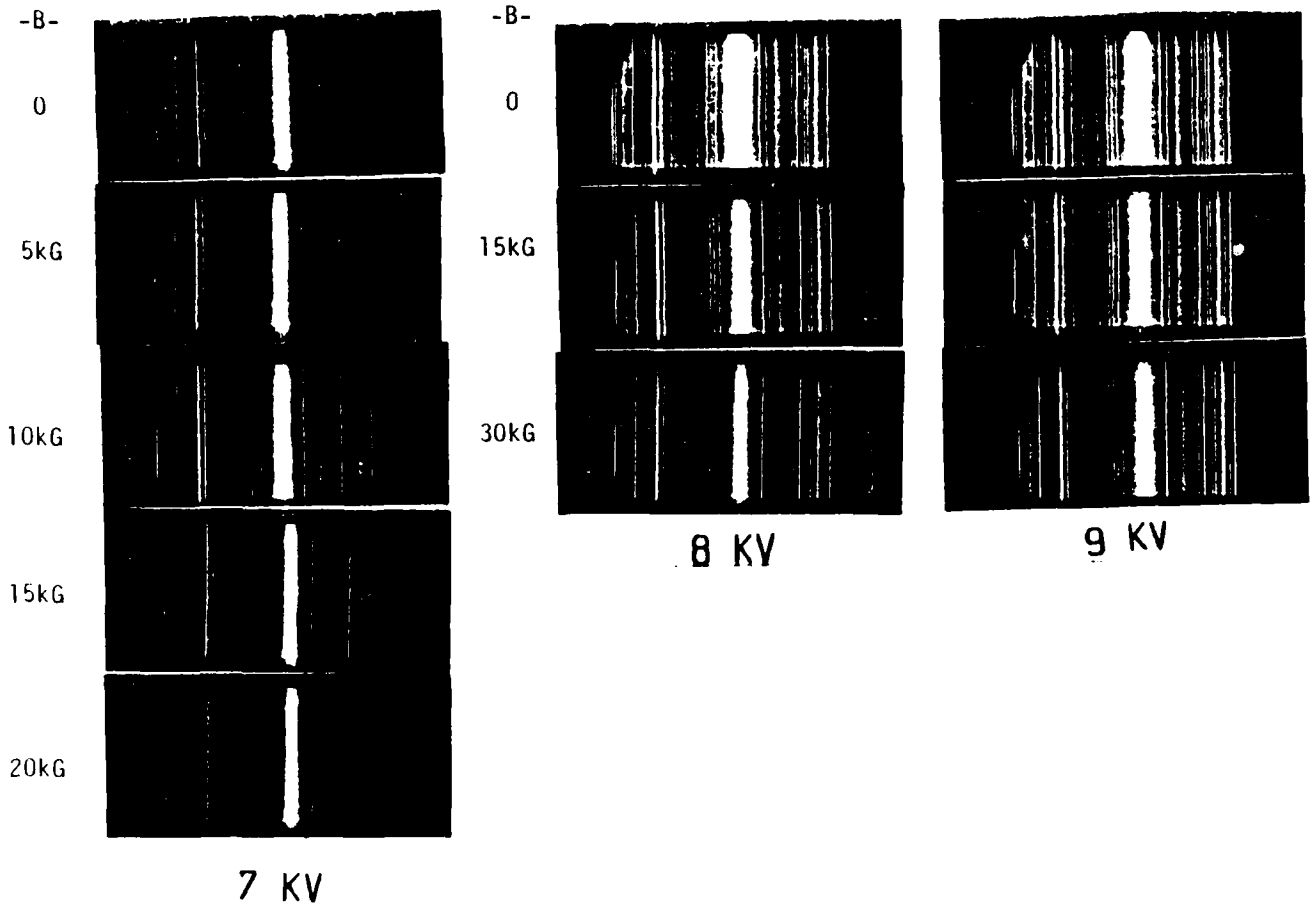

window region of the drift-tube as shown in Figure II.7. This provided a target for the plasma, and the resulting scintillation of the quartz was observed by the camera. Preliminary results are shown in Figures II.8, II.9, and II.10. A black mask covered the view-port except for a horizontal slit, and the camera streaked the image normal to that slit. As a result of placing the quartz target diagonally in the chamber (Figure II.7), the streak picture shows a different time of arrival of the plasma across the image. These preliminary results show that the plasma is relatively uniform, except for a possible m=0 oscillation.

4. B-Dot Loop Measurements

Only a limited number of B-dot measurements have been recorded. Some results are shown in Figure II.11. Detailed analysis and calculations have yet to be completed. However, from the signals recorded, it is quite clear that as the plasma enters the field, it excludes the field, but while traversing through the magnetic field region, the field is able to diffuse and is frozen into the plasma. When the plasma leaves the magnetic field region it drags some field inwards (indicated by the positive spike in signal 5 in Figure II.11. Analysis of this data allows a measurement of plasma conductivity, hence temperature, in the field region.

B. *Remaining Work During Period of Grant*

Since February 1981, an improved plasma gun (Figure II.12) has been installed in the plasma physics laboratory. The new gun was designed by Dr. M. Collins Clark based on our previous work. This gun is also capable of operating in both prefilled and puffed modes. Primary advantages are the ability to carry larger current and operate at higher gas pressure. Two puffing methods are available; the first type uses a foil (Kapton) bursting (by over-pressure) technique and the second type uses an electro-magnetically-operated puff valve. (The electromagnetic

Figure II.7. Fast Photography

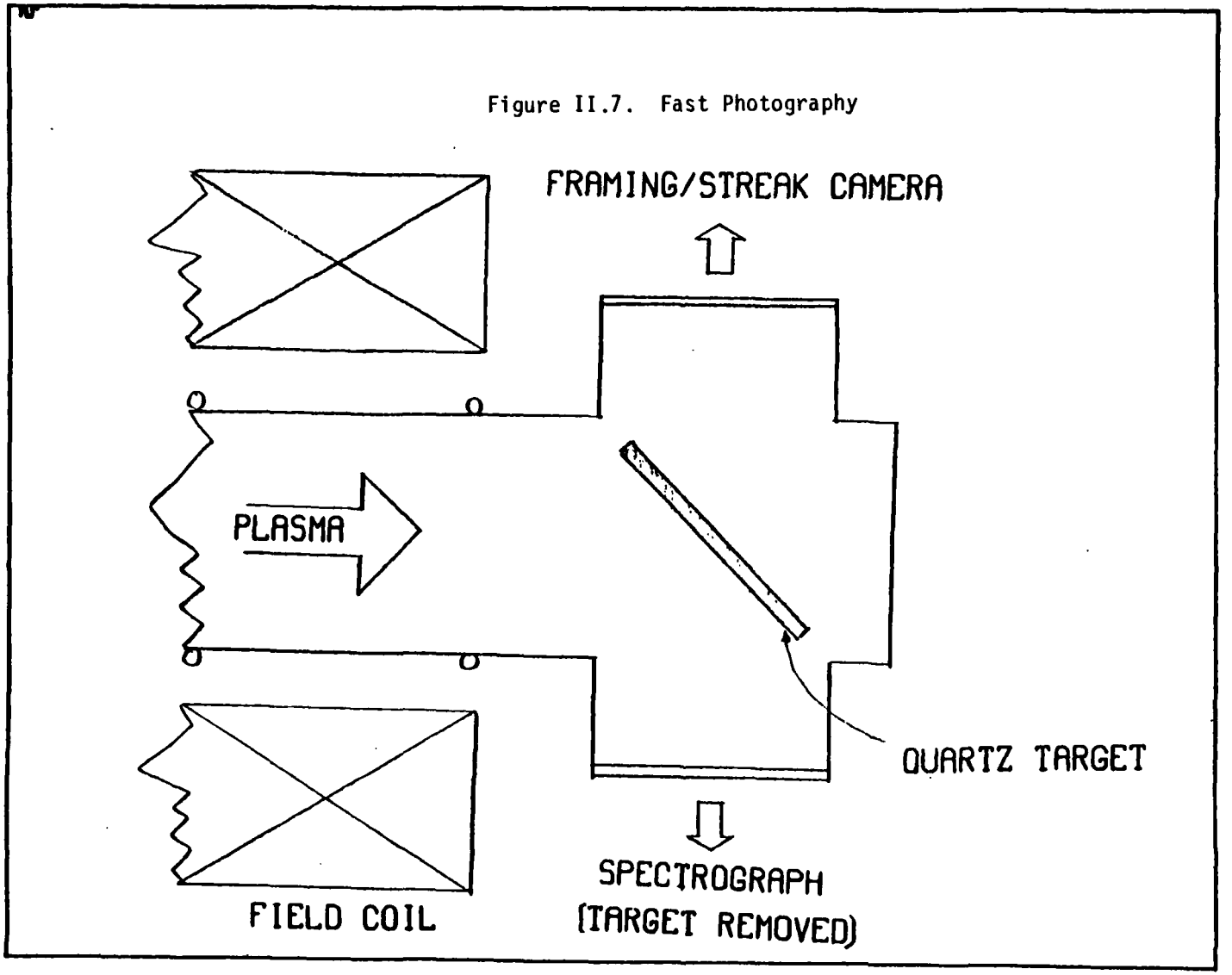

Figure II.8. Streak Photographs

SET - UP

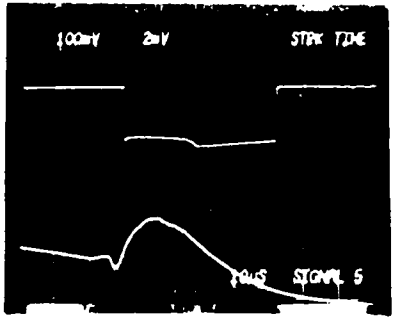

ND 1·3

SLIT

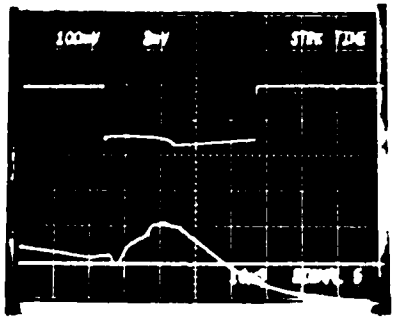

ND1·3

Figure II.9

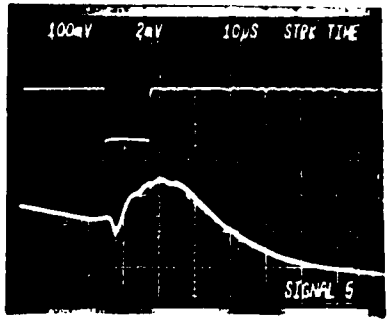

ND1·0

ND 0·3

Figure II.10. Framing Photographs

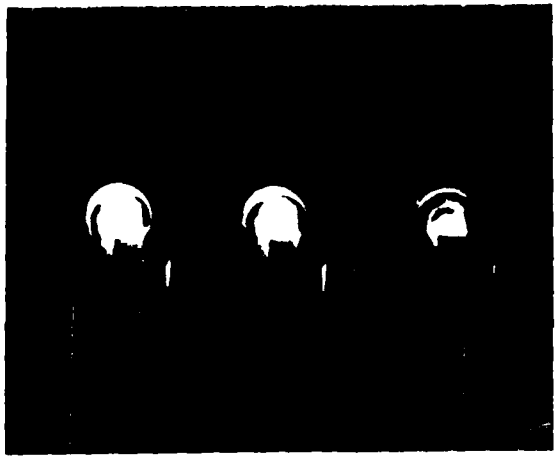

SET - UP

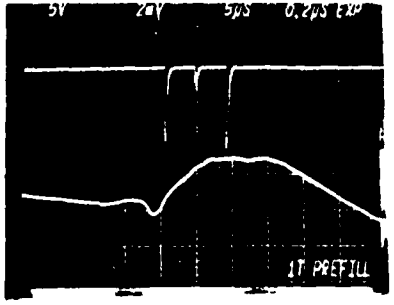

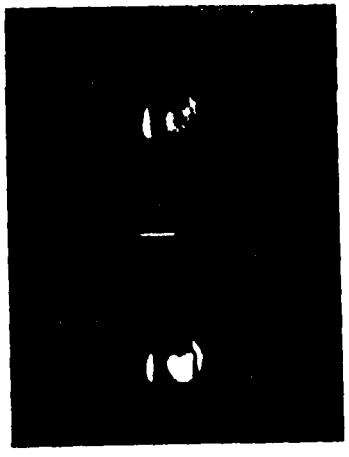

Figure II.11. B-Dot Probe Results

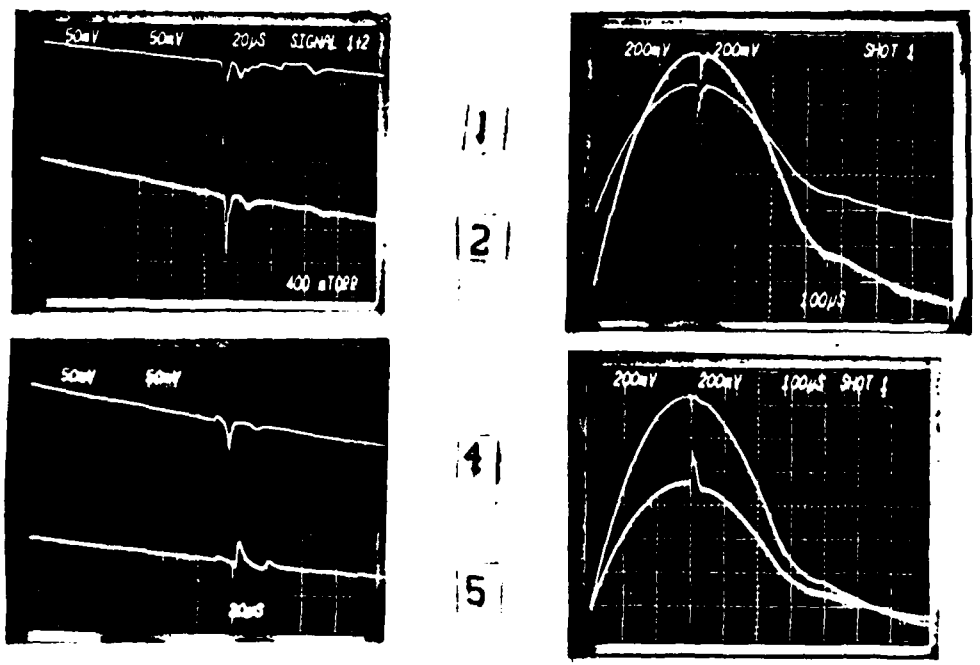

Figure II.12

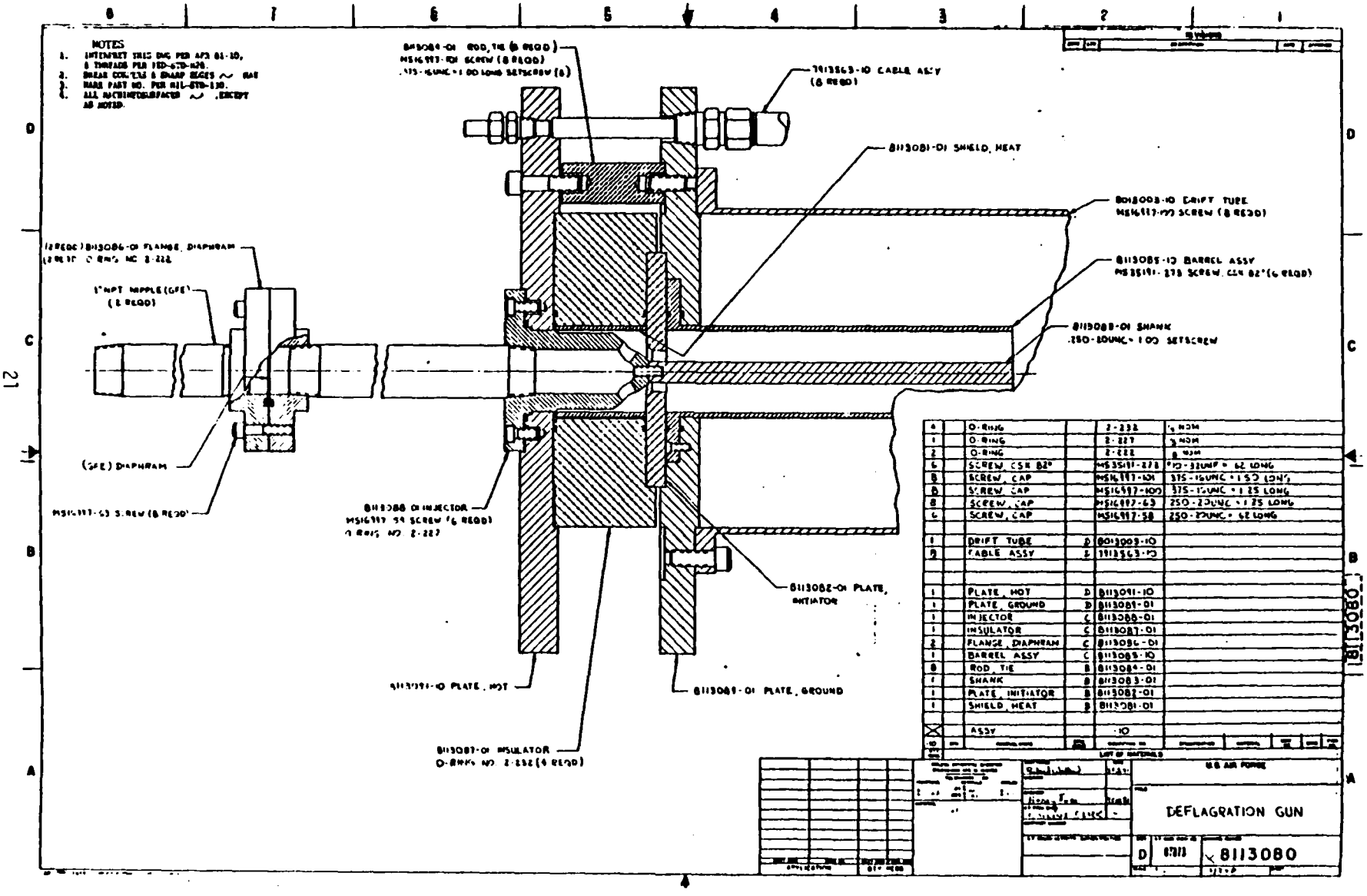
NOTES
8113084-01 ROD, TIE (6 REQD)
MS16997-101 SCREW (6 REQD)
.375-16UNC-1.00 LONG SETSCREW (6)
79113563-10 CABLE ASSY (6 REQD)
8113081-01 SHIELD, HEAT
8113083-10 DRIFT TUBE
MS16997-99 SCREW (6 REQD)
8113085-10 BARREL ASSY
MS35191-278 SCREW, CSK 82° (6 REQD)
8113088-01 SHANK
.250-20UNC-1.00 SETSCREW
(2 REQD) 8113086-01 FLANGE, DIAPHRAM
1" NPT NIPPLE (GFE) (6 REQD)
(GFE) DIAPHRAM
MS16997-63 SCREW (6 REQD)
8113088 01 INJECTOR
MS16997-99 SCREW (6 REQD)
O-RING NO. 2-227
8113082-01 PLATE, INITIATOR
8113091-10 PLATE, HOT
8113089-01 PLATE, GROUND
8113087-01 INSULATOR
O-RINGS NO. 2-232 (6 REQD)
4 O-RING 2-232 .5 NOM
1 O-RING 2-227 .5 NOM
2 O-RING 2-222 .5 NOM
6 SCREW, CSK 82° MS35191-278 .190-32UNF-.62 LONG
8 SCREW, CAP MS16997-101 .375-16UNC-1.50 LONG
8 SCREW, CAP MS16997-100 .375-16UNC-1.25 LONG
8 SCREW, CAP MS16997-63 .250-20UNC-1.25 LONG
6 SCREW, CAP MS16997-58 .250-20UNC-.62 LONG
1 DRIFT TUBE D 80139003-10
1 CABLE ASSY E 79113563-10
1 PLATE, HOT D 8113091-10
1 PLATE, GROUND D 8113089-01
1 INJECTOR C 8113088-01
1 INSULATOR C 8113087-01
2 FLANGE, DIAPHRAM C 8113086-01
1 BARREL ASSY C 8113085-10
6 ROD, TIE B 8113084-01
1 SHANK B 8113083-01
1 PLATE, INITIATOR B 8113082-01
1 SHIELD, HEAT B 8113081-01
ASSY -10
LIST OF MATERIALS
U.S. AIR FORCE
DEFLAGRATION GUN
D 8113080
80139-0181

puff valve is still in the testing phase.) Both of these are capable of delivering a large puff of neutral gas into the chamber.

In order to understand the operation of this new gun at higher total gun energy than previous work, all the diagnostics discussed above will be repeated. Furthermore, a laser holographic interferometer using a Ruby laser is currently being set up in the laboratory for measuring 2-D plasma density profiles. Other diagnostics, namely, Faraday cup, calorimeter, small magnetic probes, and electric probes will also be used on the system. Experiments involving injection of the plasma into a long drift tube with and without external magnetic field will also be continued. Some streak and framing photographs have been taken of the injection into the long transparent plastic drift tubes with a target foil/plate situated at various distances downstream. Results have not been analyzed, but will appear in our next report. A second gun has been constructed and will soon be installed on the PR 1590 REB machine to do the REB-plasma heating experiment. The presence of two identical guns in the lab will allow continued development of the source during the heating experiments. Results of that heating experiment, including plasma density and temperature measurements prior to and after REB passage, will be discussed in our final report.

III. Intense REB-Neutral Gas Heating Experiments

A. Results to Date

As a prelude to studying the interaction of a Relativistic Electron Beam with a plasma, we examined the results of beam injection into a neutral gas [8]. This section will describe those experiments, with primary emphasis on the diagnostics which were developed to examine the resulting plasma. In particular, we wished to investigate the measurement of the Stark-broadened hydrogen H_β spectral line as a beam-plasma electron-density diagnostic.

For most of these experiments, the PR 1950 (REB machine) was configured with a 5 cm diameter solid cylindrical cathode tip, a 2 to 5 cm vacuum diode gap, and a carbon-coated 25 μm thick Kapton anode foil. The polycarbonate anode foil permitted injection of the 6 MeV, 100 KA beam into a 30 cm diameter, 3 m long stainless steel drift tube backfilled with neutral hydrogen gas at pressures of one torr to several hundred torr. The low effective Z of the foil kept anode scattering, and hence beam temperature, low. In addition to the usual Rogowski coil current monitors and diode voltage monitor, a carbon calorimeter and 0.5 m visible spectrometer were routinely employed to measure transported beam energy and H_β profiles, respectively.

Stark-broadening theory for the hydrogen Balmer spectral lines is well understood [9,10] and has been verified in arc discharge experiments [11]. In particular, the H_β (2s - 4p) transition exhibits a FWHM which scales as $n_e^{3/2}$, essentially independently of temperature, over the range 10^{14} - 10^{17} electrons/cm^3 and a fraction of an eV to several eV (Figure III.1).

Furthermore, this line lies in the blue region of the visible spectrum (4861 A) and is relatively well isolated, making it an attractive candidate for an electron-beam plasma-density diagnostic. To measure the H_β linewidth a Jarrell-Ash stigmatic 0.5m spectrograph was set up to view the beam propagation channel per-

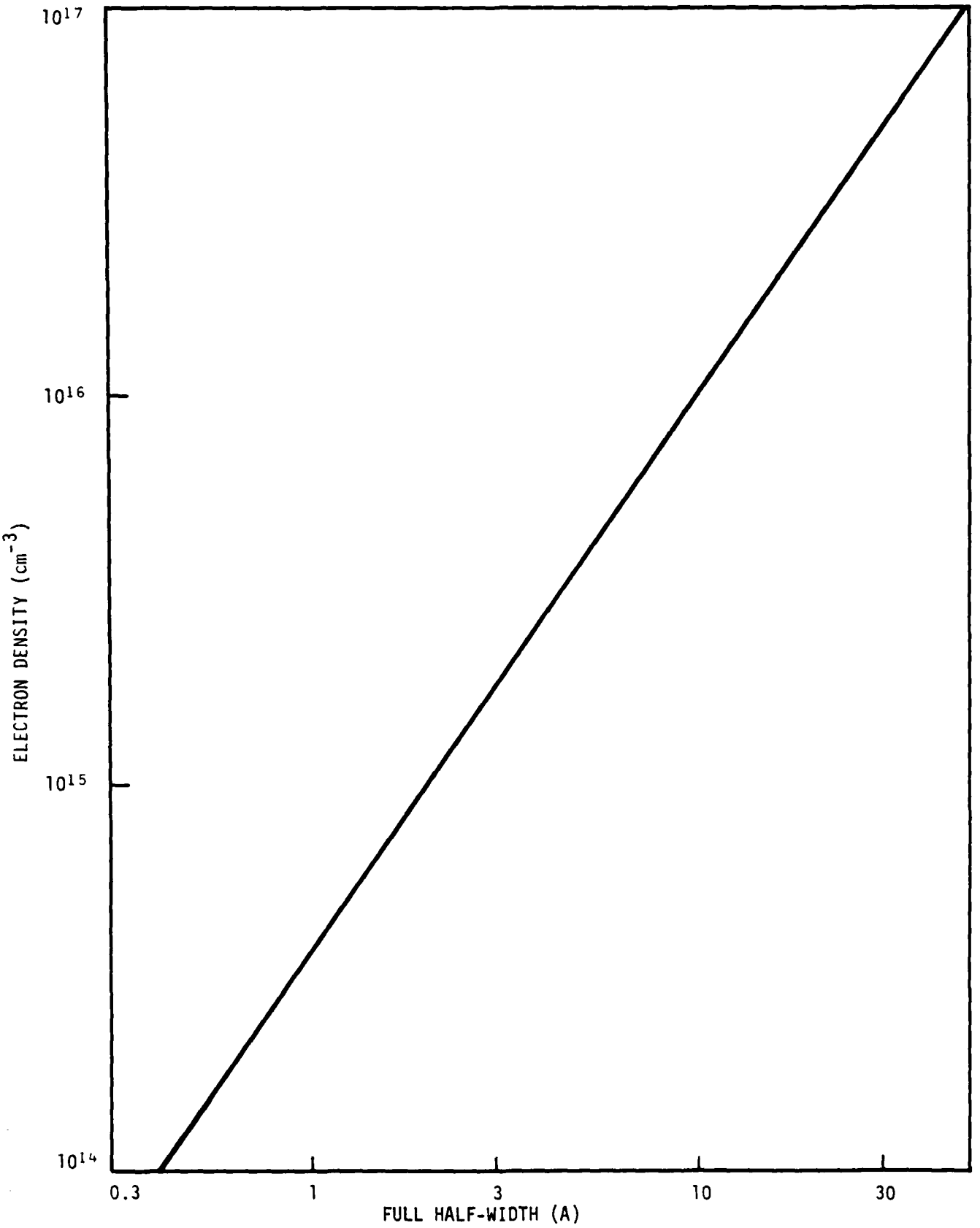

Figure III.1. Calculated half-width of the Balmer line H_β as a function of electron density for the temperature range from 5000 to 40,000 K. (from ref. 4)

pendicular to the drift tube axis (Figure III.2). The spatially-resolved H_β profiles obtained were converted to radial profiles via an Abel inversion [13], and the half-widths used to determine radial electron-density distributions.

1. Spatially-Resolved Stark-Width Measurement Technique

Preliminary to taking data, the spectrograph was aligned according to the procedures outlined in the factory manual. In addition to adjusting the focus and optimizing the resolution, the variable entrance slit width was calibrated using the diffraction pattern produced by a He-Ne laser. For most experiments, the slit was set at 200 μm, giving an instrument resolution of approximately 3 A. Kodak Royal X-Pan 4 x 5 in. cut film was selected to record the spectra because of its high sensitivity. The film speed was pushed by development for 4 min in the Kodak D-19 developer. The spectrograph exit plane dispersion and relative film response were measured in situ using a neon calibration lamp at several wavelengths near hydrogen H_β. The instrument dispersion was found to be 16.06 A/mm in the vicinity of 4861 A. To determine the relative film response, the calibration spectra for different exposure times were scanned with a diffuse microdensitometer (Perkin-Elmer). The relative exposures, in optical density units above background fog, were found to obey the simple empirical relationship

$$D = a + b \ln t , \qquad (1)$$

where D is in optical density units, t is the exposure time in seconds, and the parameters a and b were determined from linear least-squares fitting of the data. Table 1 shows the values of the fitting parameters obtained at selected NeI wavelengths. From these values, a and b for the H_β line at 4861 A were estimated to be -0.43 and +0.2, respectively.

To match the f/8 numerical aperture of the spectrograph, external optics consisting of two 45° mirrors and an apertured

λ (Å)	a	b
4715	-.2207	+.2284
4837	-.3438	+.2243
4876	-.4826	+.1964
4914	-.3775	+.2426
5031	-.3609	+.2728
5037	-.1290	+.4460

Table 1. Fitting parameters for Kodak Royal X-Pan relative film response at selected wavelengths.

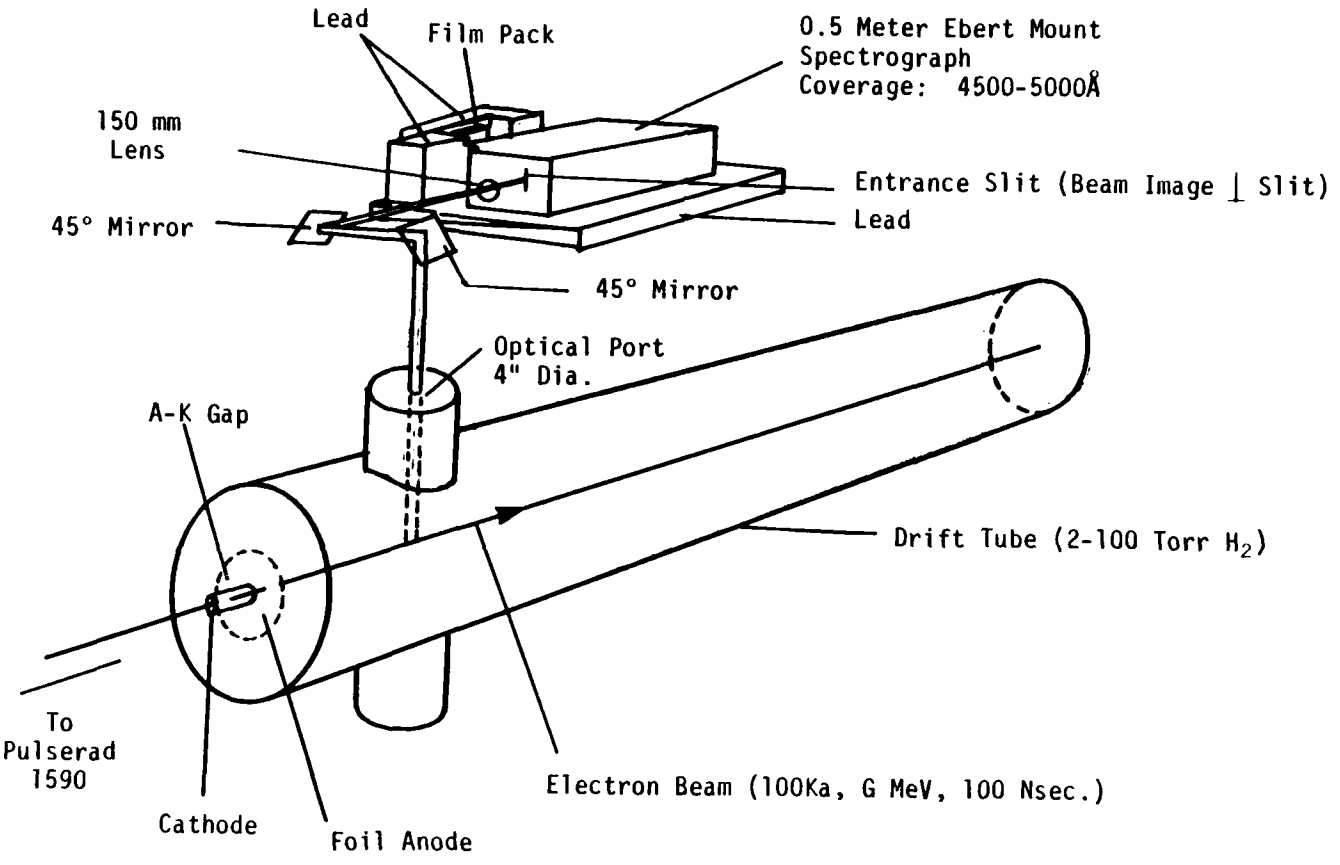

Figure III.6. Spectrograph Setup

150 mm focal-length lens were used to image a 1.5 mm long section of the plasma channel onto the entrance slit with a magnification of 0.14.

A carbon calorimeter located at the end of the drift tube and Rogowski coils mounted along the inside of the tube measured transported scan energy and net beam current, respectively. Additionally, for several shots, a plastic witness foil was taped to the anode to record the injected beam intensity pattern.

H_β spectra were recorded at fill pressures of 1, 2, 5, 10, 20, 50, 100, and 200 torr. A typical record is shown in Figure III.3. Determining the radial electron density profile from such a record involved the following steps. First, the record was microdensitometered and the optical density stored as a function of position in a 200 by 100 array on magnetic tape. The microdensitometer spot size was 100 μm square, and the resulting image field was 2 cm in the spatial (x) direction and 1 cm in the dispersion (y) direction. Next, the data was transferred to a PDP 11 data file for interactive analysis performed by a sequence of processing subroutines. The first of these scanned the data field and subtracted out the background fog density. The next converted optical densities to relative spectral intensities, I(x,y), using the film response calibration information of Equation (1). At this point it was necessary to transform the spatial intensity profiles to radial emissivity profiles by Abel inversion. Since the H_β line is an optically thin transition, the intensity of the line at the detector (entrance slit) is the line integral across chords of emitting disk as shown in Figure III.4. If the emissivity is assumed to be azimuthally uniform, the intensity is given by

$$I_y(x) = 2\int_0^{(r_o^2-x^2)^{1/2}} \varepsilon(r)\, dz = 2\int_x^{r_o} [r\varepsilon(r)/(r^2 - x^2)^{1/2}]\, dr ,$$

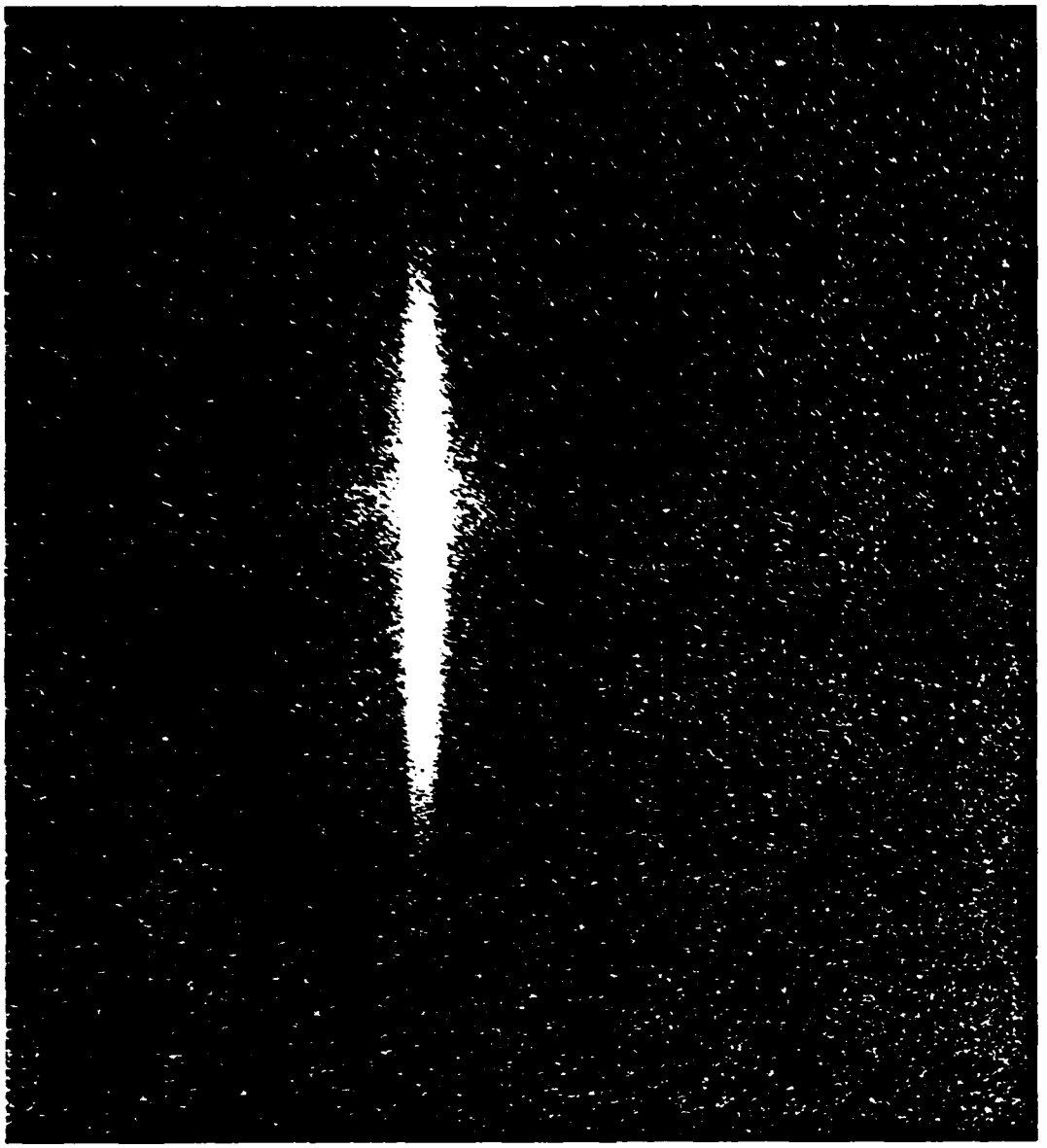

Figure III.3. Typical H_2 record.

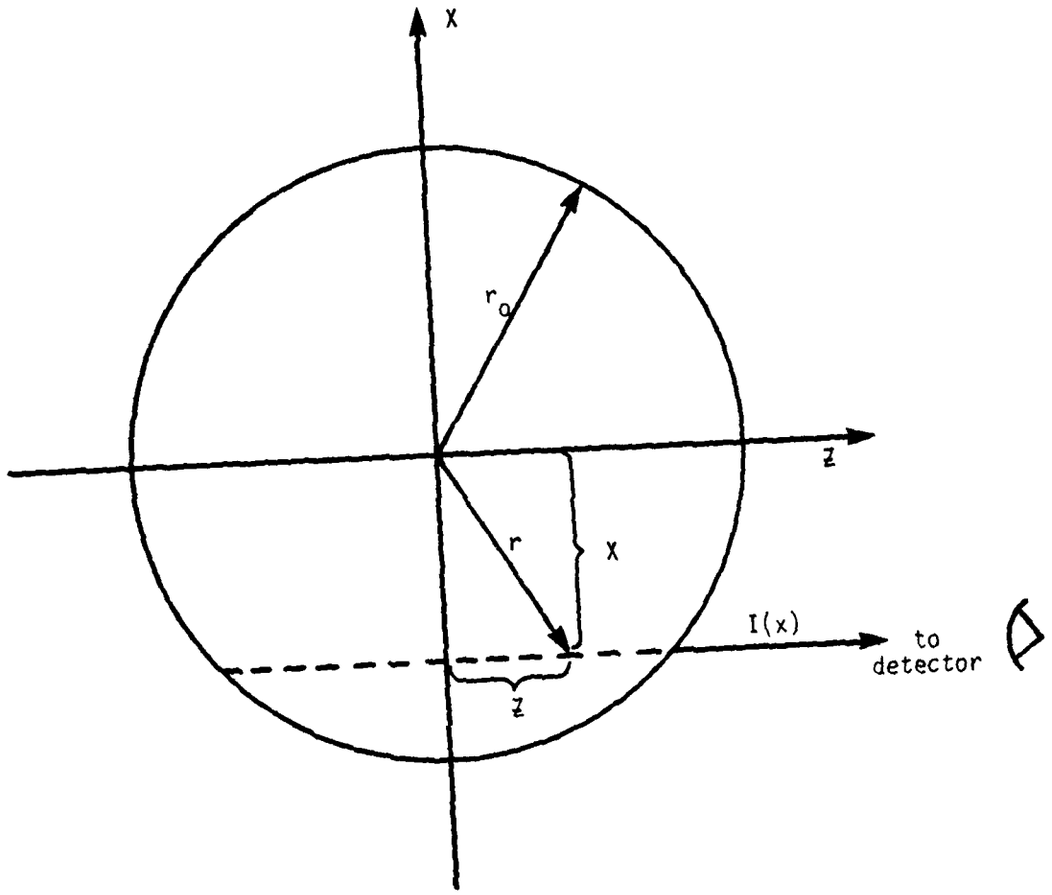

Figure III.4. Geometry for Abel inversion integrals

where ε is the emissivity, r_o is the plasma radius, and the plasma is observed in the z direction. The radial emissivity profile is then given by the Abel inversion integral,

$$\varepsilon(r) = -\frac{1}{\pi}\int_{r}^{r_o} \frac{dI(x)/dx}{(x^2 - r^2)^{1/2}}\, dx \ . \qquad (3)$$

Thus, at each wavelength location (y location on the film), the spatial (x) intensity distribution had to be inverted according to equation (3). This was accomplished by first calling a subroutine which fits a polynomial to the data $I_y(x)$,

$$I_y(x) = \sum_{k=0}^{N} c_k x^k \ , \qquad (4)$$

where N was determined by minimizing the reduced chi-squared value of the fit for $1 \leq N \leq 10$ [14]. To ease the job of fitting, the $I_y(x)$ data was split into two halves, $I_A(x)$ and $I_B(x)$, and each fit separately, as shown in Figure III.5. By comparing the two halves, we were able to check for azimuthal uniformity in a gross fashion. With $I_y(x)$ represented by polynomials, the inversion integrals were performed analytically by another subroutine which made use of formulae from tables of integrals [15]. Finally, the resultant $\varepsilon_A(r)$ and $\varepsilon_B(r)$ were reconstituted as wavelength profiles at different radii and plotted as in Figure III.6. From these profiles, the half-widths were estimated and corresponding electron densities determined and plotted.

2. Results of Measurements

Figure III.7 shows a plot of net beam current and total transported energy versus fill pressure. I_{net} is monotonically increasing with pressure, whereas energy transport is peaked at 20 torr, with significant energy transported up to 100 torr. The

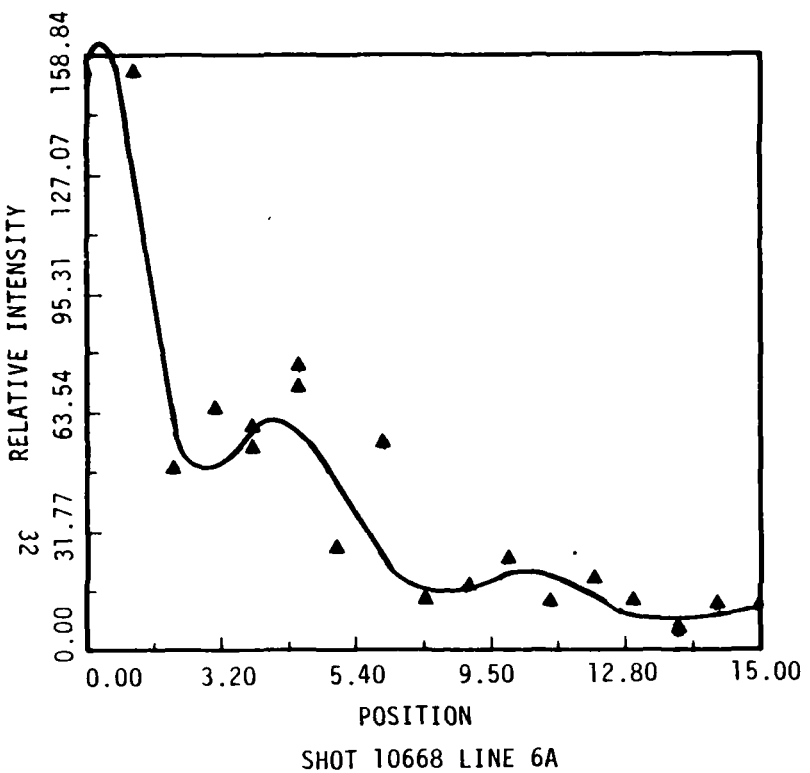

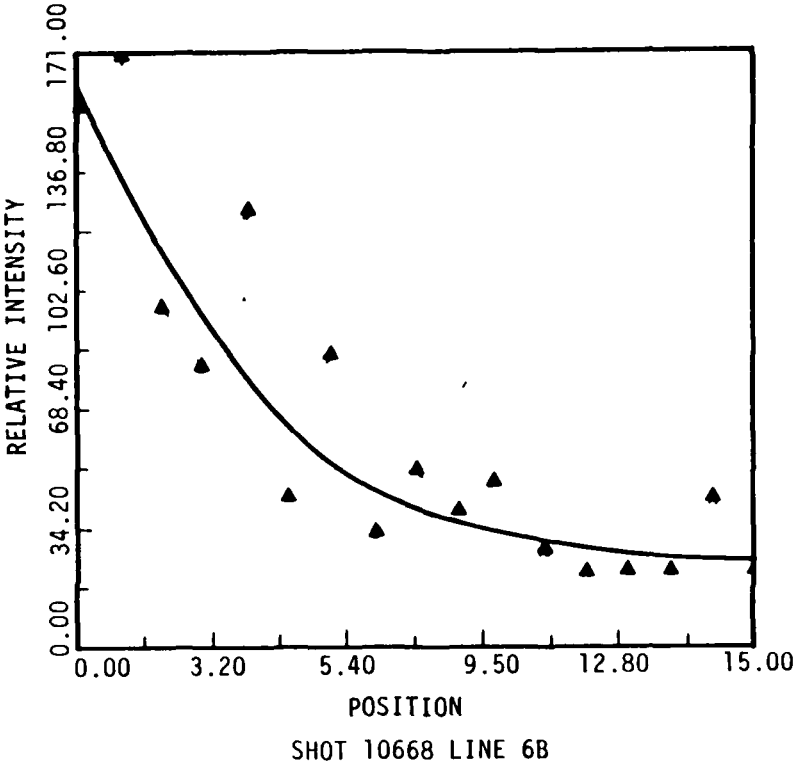

Figure III.5. Top and bottom relative intensity data and polynomial fit to data

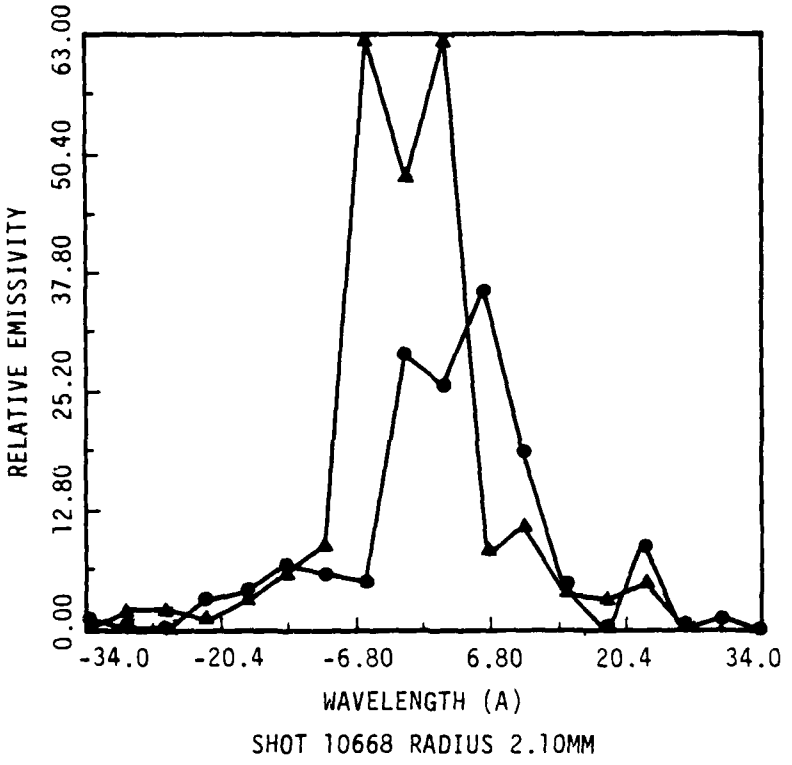

Figure III.6. Results of Abel inversion depicting line profiles for top and bottom at a radius of 2.1mm.

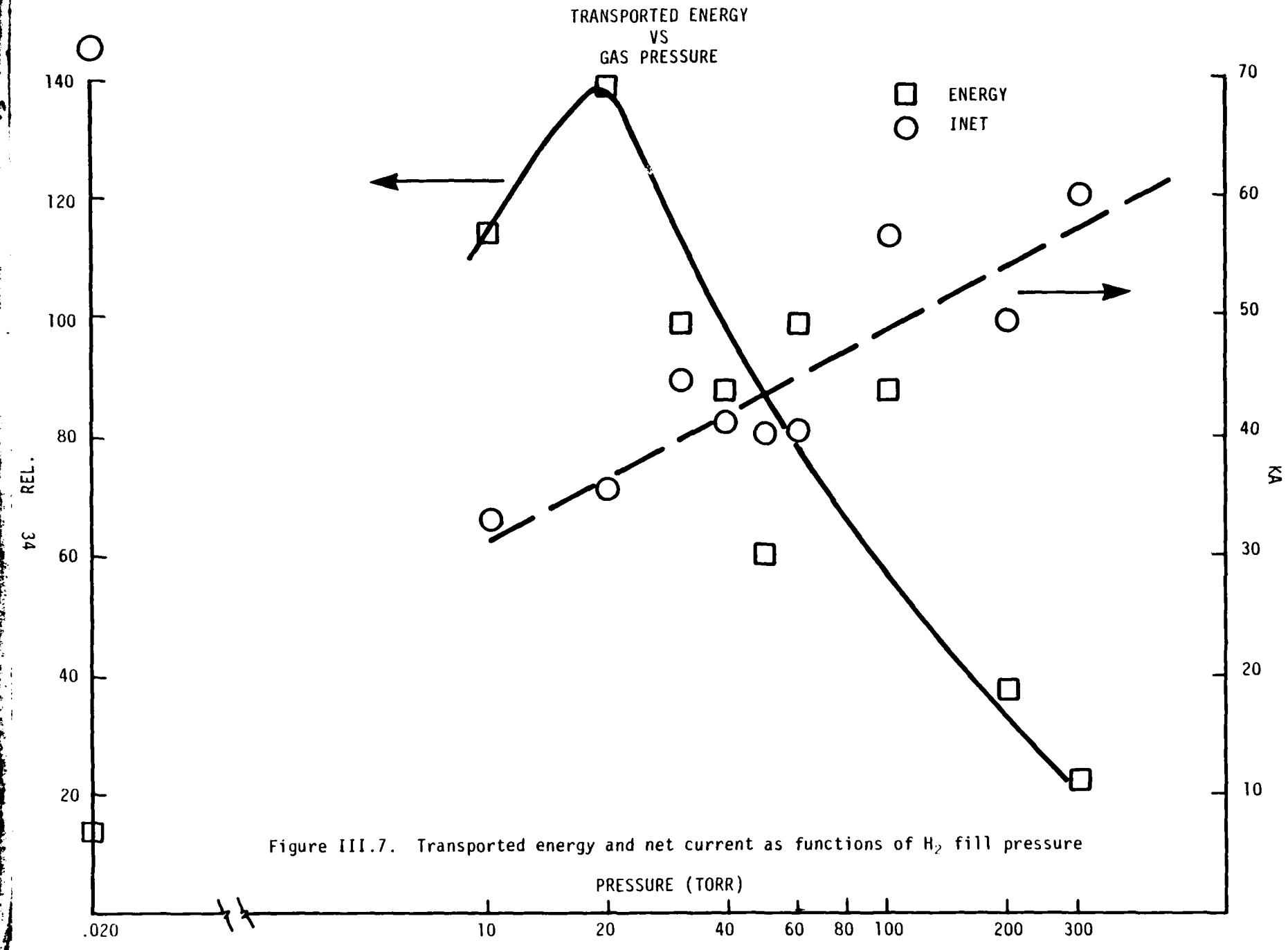

Figure III.7. Transported energy and net current as functions of H_2 fill pressure

increasing net current indicates a decreasing plasma current neutralization, as one would expect, since collision rates (and therefore, resistivity) are increasing with density. The peak in transported energy is consistent with the physical picture of a transition to quasi-stable pinched beam propagation as the current neutralization falls below the charge neutralization, allowing self-fields to create radial forces. This interpretation is substantiated by the H_β records, which show plasma diameters of approximately injection size (Figure III.8) for pressures below 20 torr, and diameters less than 1 cm for pressures of 20 torr and higher.

Finally, the results of the Stark-broadened profile analysis for the 20 torr shot are shown in Figure III.9. Although there is significant scatter in the interpreted densities, one may infer a peak density of slightly greater than 10^{16} electrons/cm^3, or about 1 percent of the hydrogen atom number density for a room temperature fill of 20 torr. Similar values of peak n_e were obtained up to 100 torr, after which the line intensities were too low to allow quantitative analysis.

Although the analysis technique described above usually produced believable electron density estimates, there were cases for which the Abel-inverted H_β line profiles bore little or no resemblance to any realistic profile. This was especially true in the line wings and plasma boundaries where intensities were low and signal-to-noise ratios poor. It has recently been suggested that an improvement in the Abel inversion can be achieved by using a cubic spline fit minimizing variations in the first derivative for the spatial intensity data rather than using a polynomial fit [16]. It may be, however, that these experiments are inherently azimuthally nonuniform and, therefore, inappropriate for Abel inversion at all [17]. Perhaps, in this case, the superposition of data from many cumulative shots could be used to obtain average density profiles.

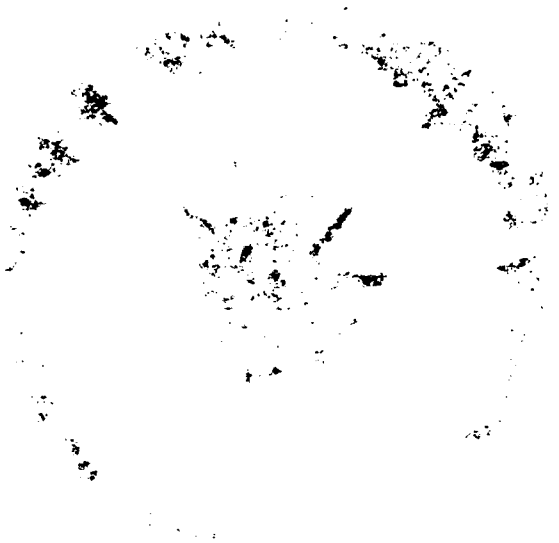

Figure III.8. Contact print of anode witness foil.

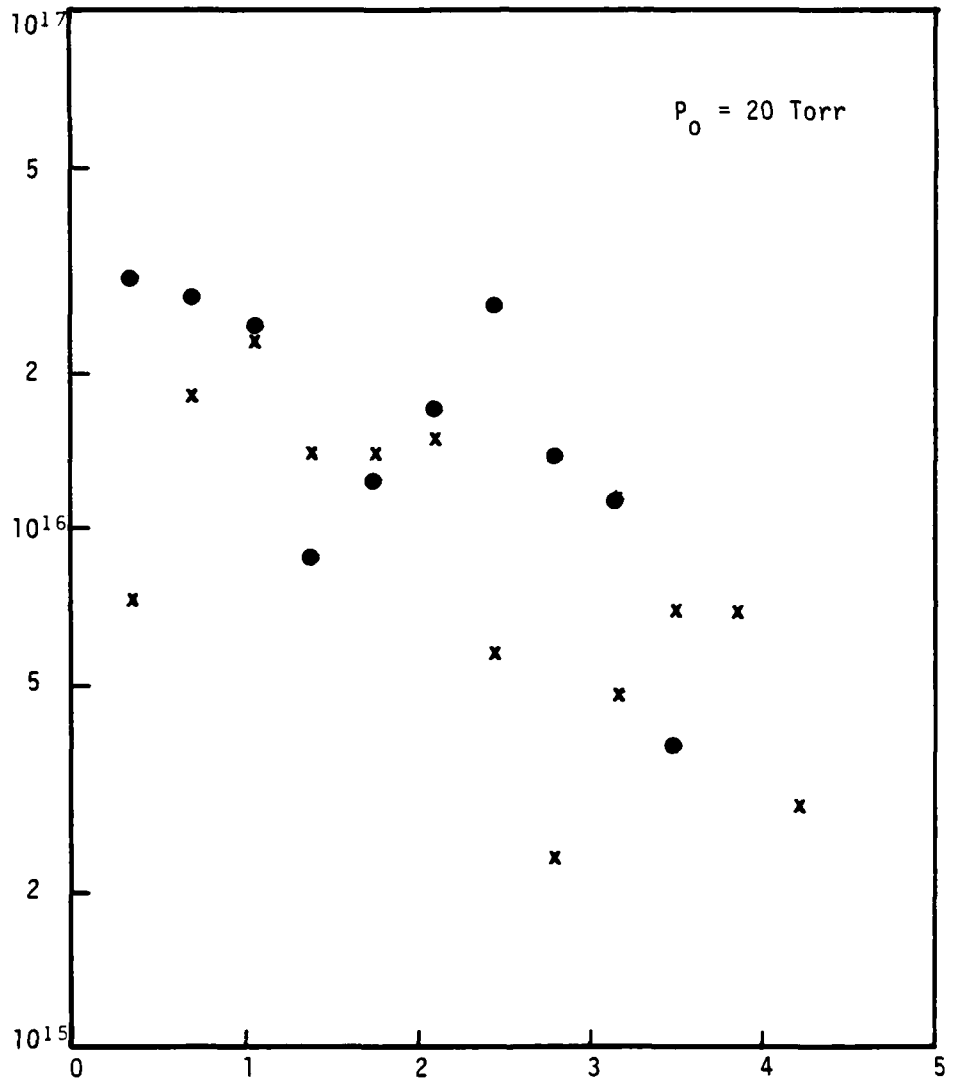

Figure III.9. Top (x) and bottom ( ) radial density profiles interred from Abel inverted relative H_3 intensity data for 20 torr shot.

Another problem which needs to be addressed is the time history of the line emission. That is, the spectrograms recorded in these experiments were time-integrated, and, at best, represent a crude weighted average description of complex time-dependent phenomena. An independent time and space resolved measurement such as infrared interferometry would be useful in ascertaining the validity of this diagnostic technique.

B. Remaining Work during Period of Grant

The REB-neutral gas experiments were a useful exercise for checking out spatially-resolved plasma density measurements. Calorimeter and Rogowski diagnostics allow beam energy deposition efficiency to be computed. All of these diagnostics, as well as additional plasma temperature measurements will be fielded for the REB-plasma heating experiments to be done in the final year of our grant.

IV. Diagnostic Development for X-Ray Simulation Source (SHIVA)

The Air Force Weapons Laboratory is continuing to develop and investigate imploding liner plasma generation, experimentally and theoretically [18]. The present experiments involve discharging a 226μF, 100-200 KV, 1.4 μsec capacitor bank through a 70 mm radius by 20 mm long cylindrical foil (120-300 $\mu g/cm^2$ aluminized formvar $\{C_5H_8O_2\}$) in a low inductance (3 nH) vacuum diode. Typical discharge parameters are: peak current of 10-12 MA, 1.2 to 1.8 μsec current rise time, 1.2 to 1.8 μsec implosion time, and peak electrical power of 0.7 Terrawatts. Radiation pulses (assuming isotropic emission) as large as ~250 KJ with pulse widths (FWHM) ranging from 80 to 200 nsec and rise times as short as 40 nsec are obtained.

In this report, we discuss spectral and spatial data obtained with a grazing incidence spectrograph. The particular SHIVA experiments on which the spectrograph data were taken were 100 KV, 1.3 MJ implosions of 160 $\mu g/cm^2$ foils. The radiation output (isotropic assumption) was ~100 KV and ~100 nsec, and time-resolved, filtered X-ray photoelectric diode measurements were made for comparison with the grazing incidence spectrograph results.

The imploding liner chamber and X-ray diagnostic geometry are illustrated in Figure IV.1. Chamber design limits diagnostic access to the axial direction. Since blast and debris from the experiment are significant, passive diagnostics require the use of fast closure shutters. Two types of shutters were used in series to protect the grazing incidence spectrograph. The slow shutter is a pneumatic piston-blade shutter which closes a 10 mm gap in ~600 μsec [19]. The fast shutter uses a 240 μF, 5 KV, 7 μsec rise time bank to theta-pinch a 25 mm diameter, .25 mm wall aluminum cylinder [20].

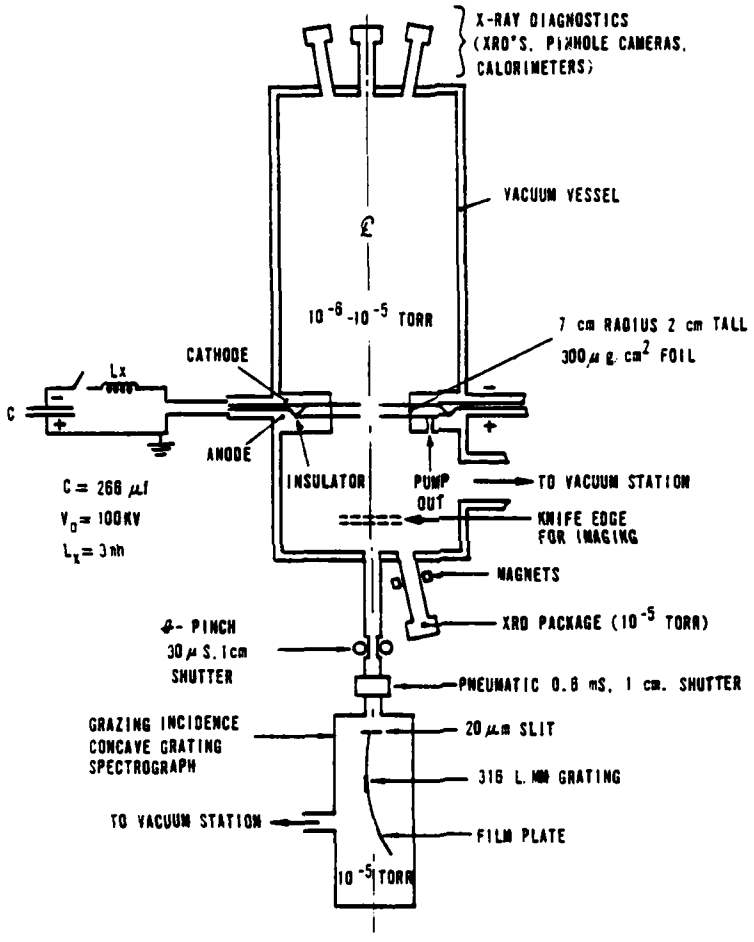

Figure IV.1

SCHEMATIC OF SHIVA DIAGNOSTIC GEOMETRY
WITH GRATING SPECTROGRAPH
(NOT TO SCALE)

The grazing incidence spectrograph detailed geometry and useful relations are indicated in Figure IV.2. The instrument was purchased from Grazing Measurements Limited [21] and has the following parameters. A micro-machined Rowland circle and precision-manufactured, factory-aligned, X-ray phase lamellar gratings provide ease of alignment and rapid grating interchange. Using a grazing incidence angle of 0.5-4.0 degrees, the 316 1/mm concave grating (5 m radius of curvature) allows a wide range of energy coverage. A precision adjustable entrance slit and emulsion plate holder make up the remaining components of the spectrograph. A separate spectrograph vacuum pump allows the system to be maintained at 5×10^{-6} Torr during an experiment, independent of the main chamber vacuum. For the particular experiment described here, the grating-plate and grating-entrance slit distances were 0.25 m and 0.18 m, respectively, yielding a grazing angle of 2.5 degrees and an energy coverage of 80 to 580 eV in first order. The photographic plates used for spectral recording were Ilford Q2 plates. Calibrations of Hobby and Peacock [22], as well as our in-house calibrations were used to compute system response. The grating reflectivities were independently measured at the National Physical Laboratory at Imperial College, London, England [23].

In order to obtain time-integrated, spatial profiles of the emitting plasma region, and imaging knife edge was used with the grazing incidence spectrograph. Penumbral analysis of images occluded by such an imaging element allow a spatial emission profile to be obtained. We have previously reported [24] the use of such a technique with bent crystal spectrographs. The position of the imaging knife edge is shown in Figure 1. Note that the knife edge perpendicular to the entrance slit of the spectrograph. Thus, the image information is stored in the non-dispersive direction on the plate.

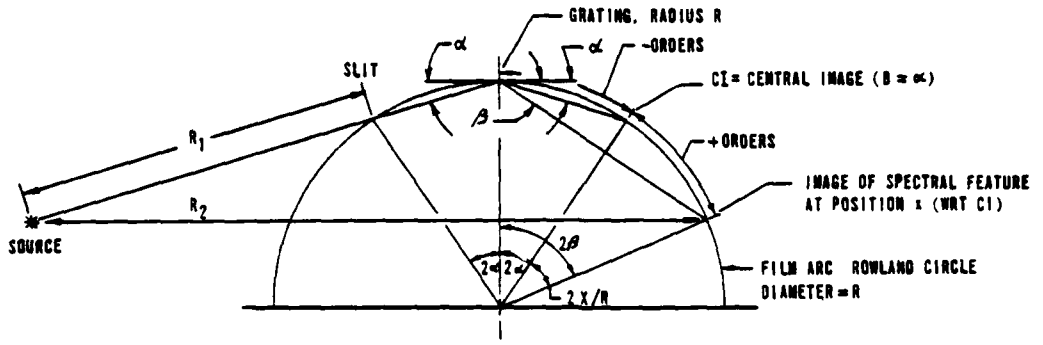

$$m\lambda = d\ (\cos\alpha - \cos\beta)$$

$$\frac{dW}{dh\nu} = (4\pi R_1 R_2) \left(\frac{D}{wG_\nu P_\nu}\right) \left(\frac{dx}{dh\nu}\right)$$

$$\frac{dh\nu}{dx} = \left(\frac{hc}{\lambda^2}\right) \left(\frac{d \sin\beta}{mR}\right)$$

$$\frac{dW}{dh\nu} = (4\pi R_1 R_2) \left(\frac{D}{wG_\nu P_\nu}\right) \left(\frac{1}{hc}\right) \left(\frac{mR}{d \sin\beta}\right) \left[\frac{d}{m} (\cos\alpha - \cos\beta)\right]^2$$

where

D = optical density

w = slit width

G_ν = grating efficiency

P_ν = film sensitivity

h = Planck's constant

c = speed of light

$h\nu$ = photon energy

W = isotropic total source emission

Figure IV.2

GRAZING INCIDENCE CONCAVE GRATING SPECTROGRAPH AND RELATIONS

A positive print of the spectrograph plate obtained on the SHIVA shot is shown in Figure IV.3. An entrance slit of 20 μm was used, along with a light filter of 50 $\mu g/cm^2$ carbon. The spectrum shown runs from 80 eV to 580 eV in first order. It is noteworthy that the spectrum below about 120 eV is dominated by continuum, the spectrum above C-K_α (284 eV) is dominated by emission lines, and the region between these points is continuum, overlaid with strong absorption lines. A microdensitometer scan of the data is shown in Figure IV.4. There is a strong absorption feature at Carbon K_α, characteristic of the light filter used on the experiment. There are roughly 30 emission lines which are identified in Table 1. A number of the more intense absorption lines are identified in Table 2.

The emission spectrum is primarily due to Al^{+10} and C^{+5} with components of O^{+6} and other high ionization states of Al. These are characteristic of a 100-200 eV plasma. Previously reported bent crystal spectrograph data on similar shots indicated an emitting region density of ~10^{20} cm^{-3}, 150-200 eV, few mm diameter core, surrounded by a 10^{20}-10^{21} cm^{-3}, 250-300 eV, ~1 cm^3 region, which is in turn surrounded by a lower density, ~40 eV, few cm^3region. The higher temperature regions of the plasma would be responsible for the emission lines seen in the grazing incidence spectrum. Typical line widths of the C^{+5} (C-VI) 1s-np series is shown in Figure IV.5. Following computations of Kepple and Griem (Reference 28), we estimate that these lines were emitted from a region of electron density $(n_e) \leq 4 \times 10^{20}/cm^3$. Another series also shown is the 2s-np series from Al^{10+} (Al-XI). Estimates of linear Stark broadening indeicate a density $(n_e) \geq 10^{22}/cm^3$. Thus we conclude the brightly emitting Al^{10+} and C^{5+} are in different regions (densities) of the plasma. This is consistent with the 2D-MHD computational results.

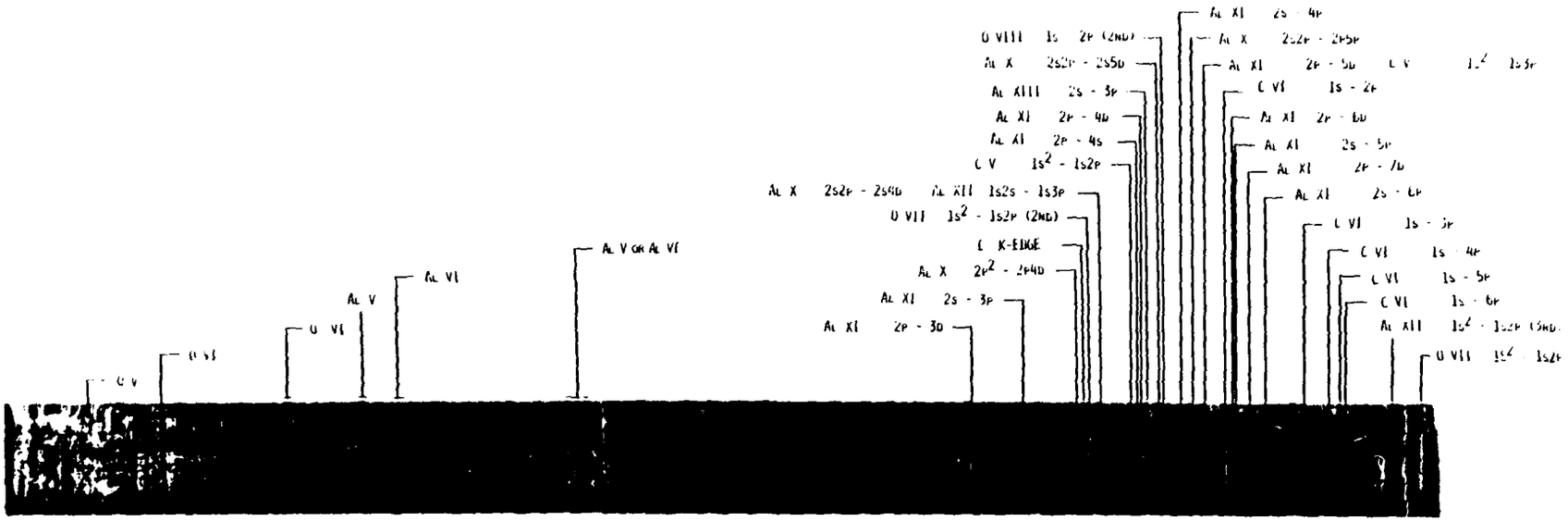

Figure IV.3. SHIVA 4040 Grazing Incidence Spectrum

Figure IV.4(a). SHIVA 4040 Grazing Incidence Spectrum Microdensitometer Scan

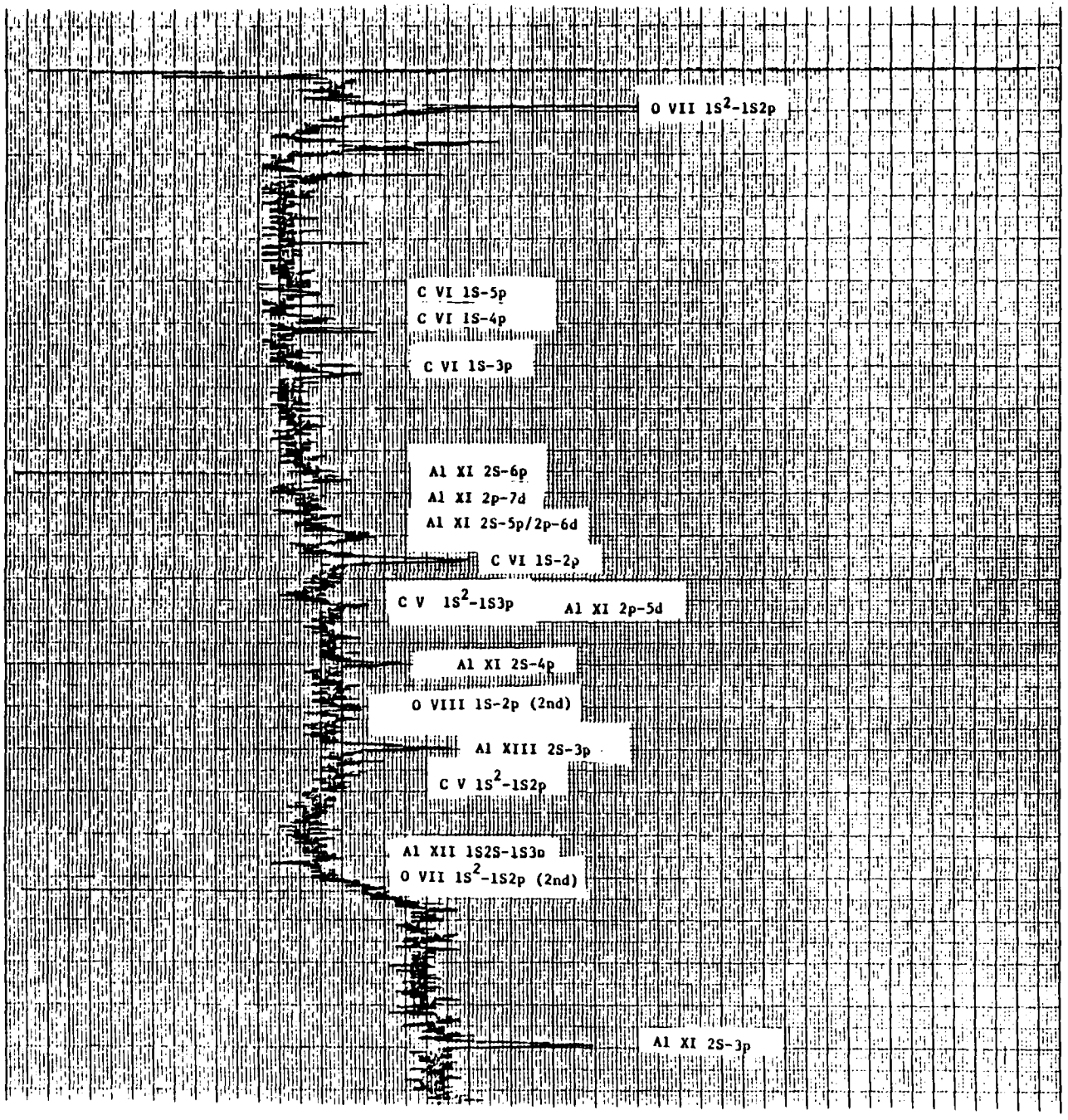

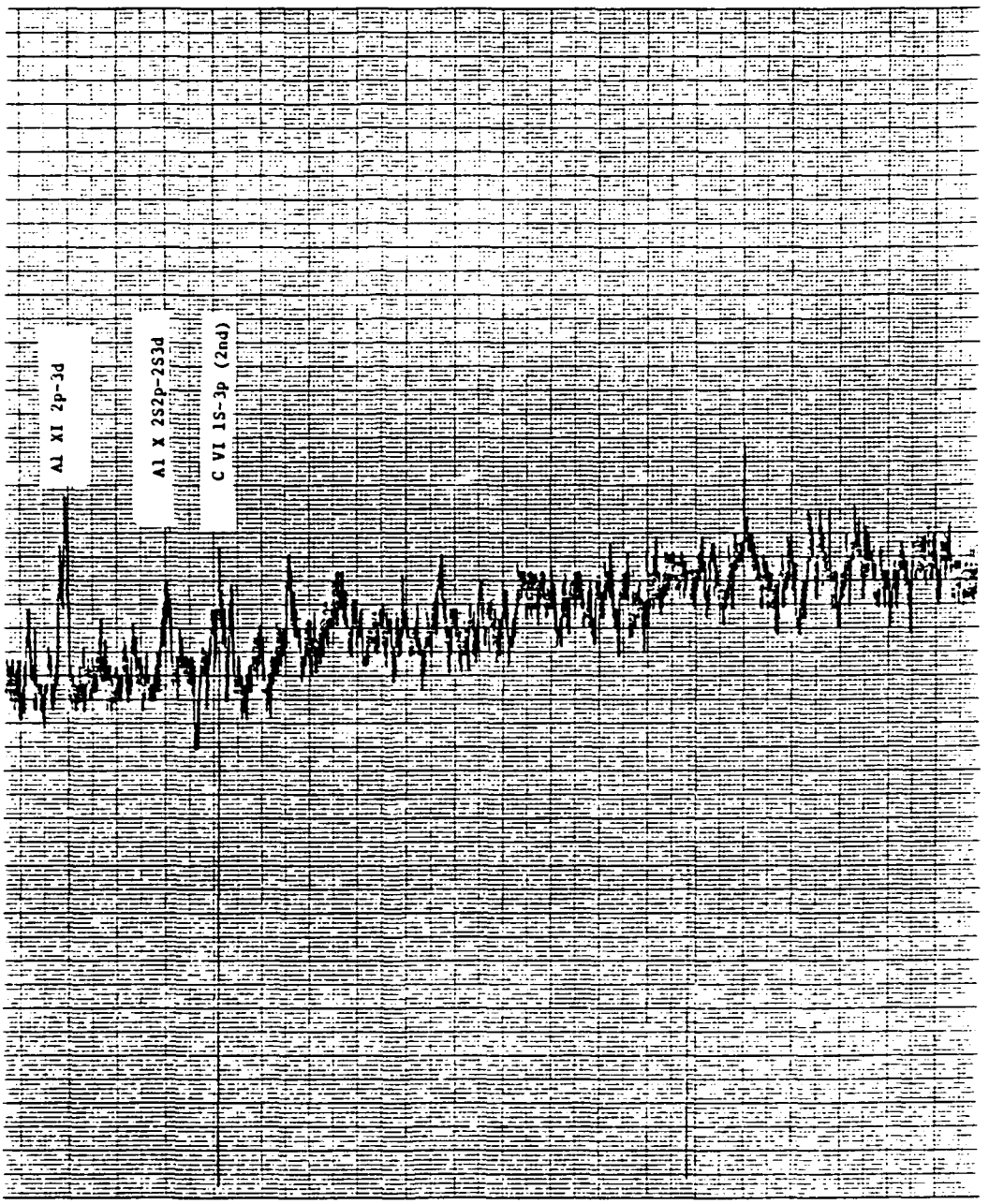
HEWLETT-PACKARD 9270-1037
Al XI 2p-3d
Al X 2S2p-2S3d
C VI 1S-3p (2nd)

Figure IV.4(b)

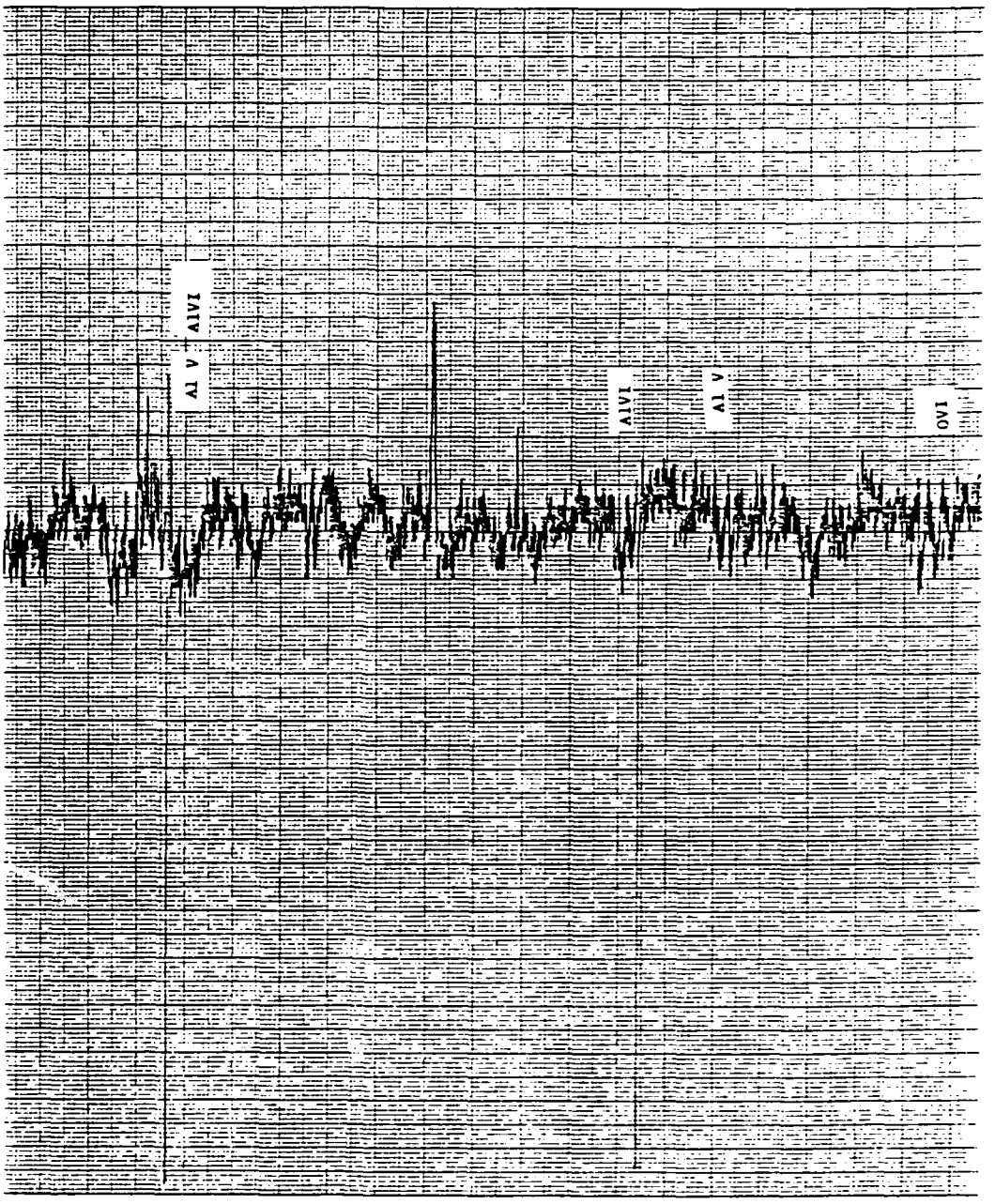

Figure IV.4(c)

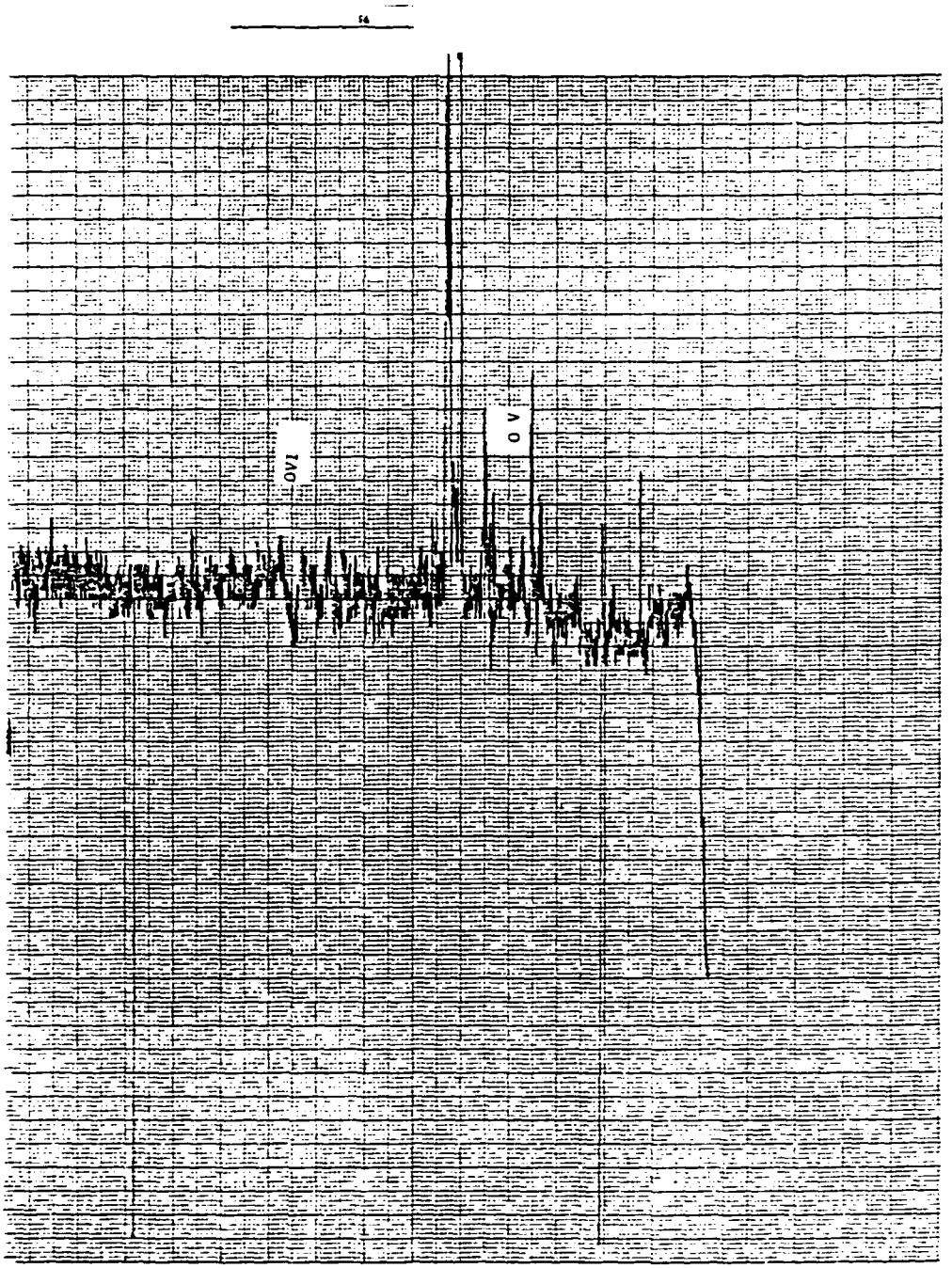

Figure IV.4(d)

Table I

EMISSION LINE IDENTIFICATION

1. O VII $1s^2$-1s2p (21.60Å)
2. Al XII $1s^2$-1s2p (7.757Å, 2nd order)
3. C VI 1s-6p (26.03Å)
4. C VI 1s-5p (26.36Å)
5. C VI 1s-4p (26.99Å)
6. C VI 1s-3p (28.47Å)
7. Al XI 2s-6p (31.31Å)
8. Al XI 2p-7d (32.13Å)
9. Al XI 2s-5p (33.01Å)
10. Al XI 2p-6d (33.17Å)
11. C VI 1s-2p (33.736Å)
12. C V $1s^2$-1s3p (34.97Å) Al XI 2p-5d (35.05Å)
13. Al X 2s2p-2p5d (35.85Å)
14. Al XI 2s-4p (36.68Å)
15. O VIII 1s-2p (18.9Å, 2nd order)
16. Al X 2s2p-2s5d (38.3Å)
17. Al XIII 2s-3p (38.73Å)
18. Al XI 2p-4d (39.1Å)
19. Al XI 2p-4s (39.52Å, 39.62Å) Al X 2s2[-2p4p (39.54Å, 39.63Å)
20. C V $1s^2$-1s2p (40.27Å)
21. Al X 2s2p-2s4d (42.34Å, 42.40Å) Al XII 1s2s-1s3p (42.23Å)
22. O VII as^2-as2p (21.60Å, 2nd order)
23. C ($k\alpha$) edge (43.66Å)
24. Al X $2p^2$-2p4d (44.49Å)
25. Al XI 2s-3p (48.34Å)
26. Al XI 2p-3d (52.30Å, 52.45Å)

Table 2

ABSORPTION LINE IDENTIFICATION

	Al VI $2p^4$-$2p^3(^2P^\circ)3s$ (103.94Å)
A1	Al VI $2p^4$-$2p^3(^2D^\circ)3s$ (104.05Å)
	Al VI $2p^4$-$2p^3(^2D^\circ)3s$ (104.34Å)
	Al VI $2p^4$-$2p^3(^2D^\circ)3s$ (104.47Å)
A2	Al V $2p^5$-$2p^4(^3P)3d$ (107.71Å, 107.94Å, 108.00Å, 108.06Å, 108.11Å, 108.32Å, 108.38Å, 108.40Å, 108.45Å, 108.46Å)
A3	O VI 2s-4p (115.82Å)
	O VI 2p-5d (116.35Å, 116.42Å)
A4	O VI 2p-4d (129.79Å, 129.87Å)
A5	O V 2s2p-2s5d (138.03Å, 138.05Å, 138.11Å)
A6	Al V or Al VI (85.6Å)
	(85.8Å)
A7	Al V or Al VI (87.0Å)
	(87.3Å)
A8	Al V or Al VI (87.4Å)

Figure IV.5. Line Widths; Stark Effect

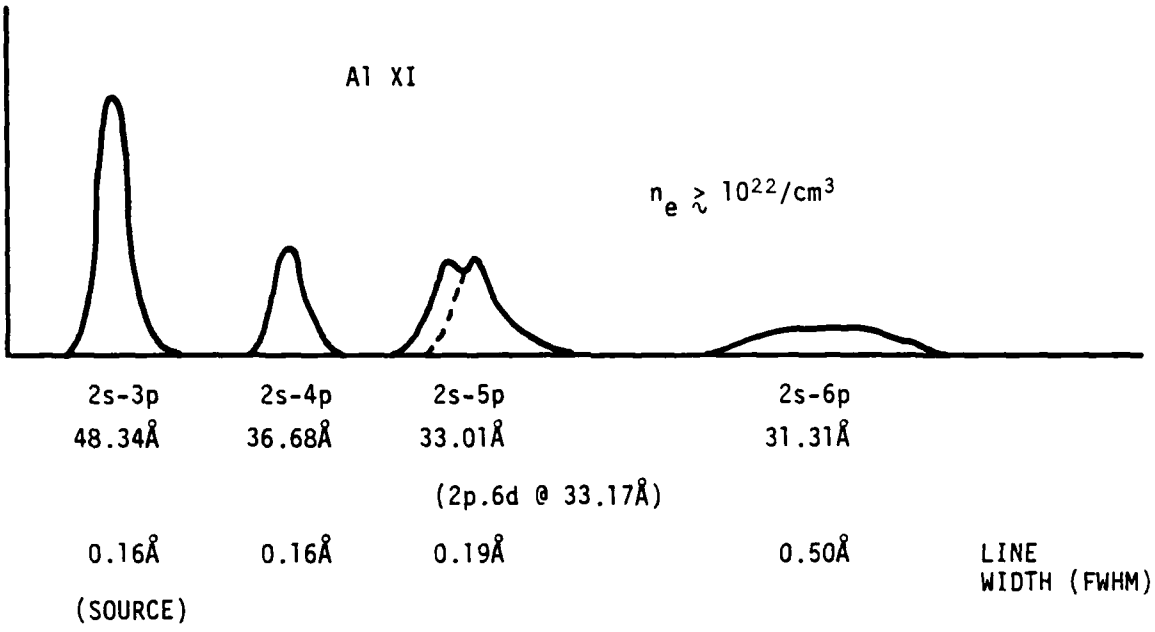

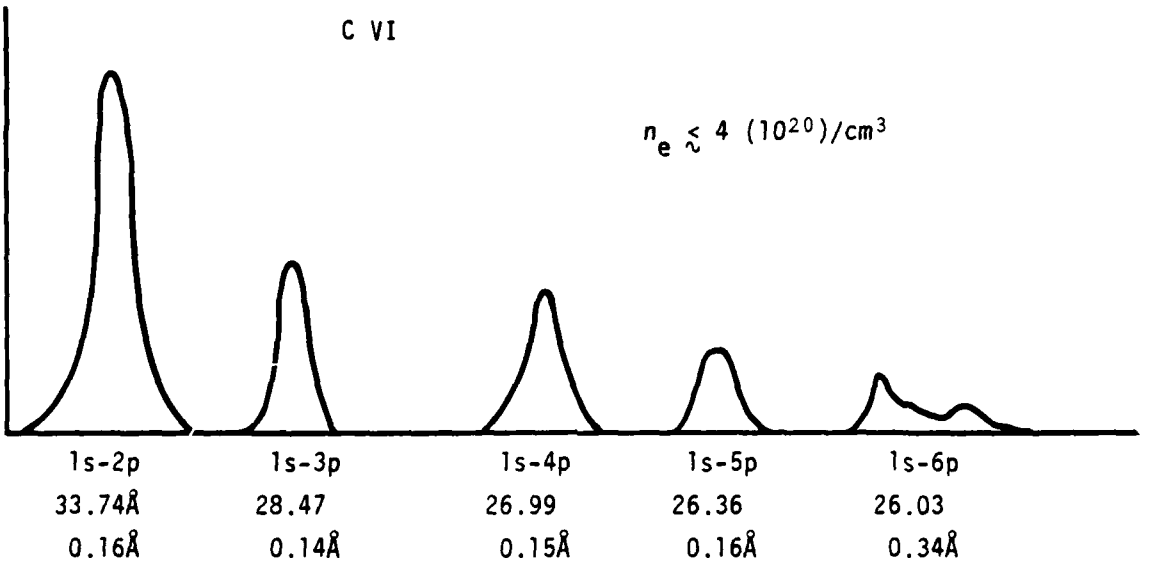

The absorption spectrum observed in this data is principally due to low ionization states of Aluminum and Oxygen (Al^{+4} and Al^{+5}; O^{+4} and O^{+5}). These lines suggest that the hot, inner plasma core is shining through a cooler, absorbing plasma envelope. The presence of a low temperature axial plasma plume was first observed in this spectrograph data, and subsequently seen in our 2D-MHD simulations. Of about 150 emission lines observed in the spectrum, we have identified roughly 100. Most belong to this group of low ionization state O and Al lines. The temperature inferred from the ionization state of these atoms is roughly 40 eV, consistent with the 2D-MHD results presented in Figure IV.6. Also consistent with this temperature is an apparent peak in the continuum at about 100 eV, although this result is tentative, pending further low energy calibration of the spectrograph system. The spectral unfold of x-ray diode data taken on the same shot is shown in Figure IV.7. A discussion of the time-resolved spectral unfold procedure was presented earlier.[27] Note the evidence of multiple temperature components, consistent with both 2D-MHD predictions and observed spectrographic data. A rough comparison of the integrated emission spectrum as measured by the grazing incidence spectrograph is also included for comparison. The absolute level of the results are awaiting further improvement in calibration at the energy levels of interest.

Some of the spatial information contained in the spectrograph data is shown in Figure IV.8. This figure displays the microdensitometer scan down the length of the Al^{+12} (2s-3p) line at 320 eV. The intensity variation indicated by the circled letter A contains the penumbral spatial profile from an imaging element (knife edge). The emitting region has a computed width of 3.3 mm. Figure IV.9 (a and b) shows the continuum scans at slightly higher and lower energies than the line in Figure IV.8. The continuum emitting regions have a computed width of 8.0 mm. Scans of other emission lines show emission regions which vary

Figure IV.6

2D-MHD PREDICTIONS OF IMPLODING LINER PINCH STRUCTURE AT REPRESENTATIVE TIME DURING RADIATION PULSE

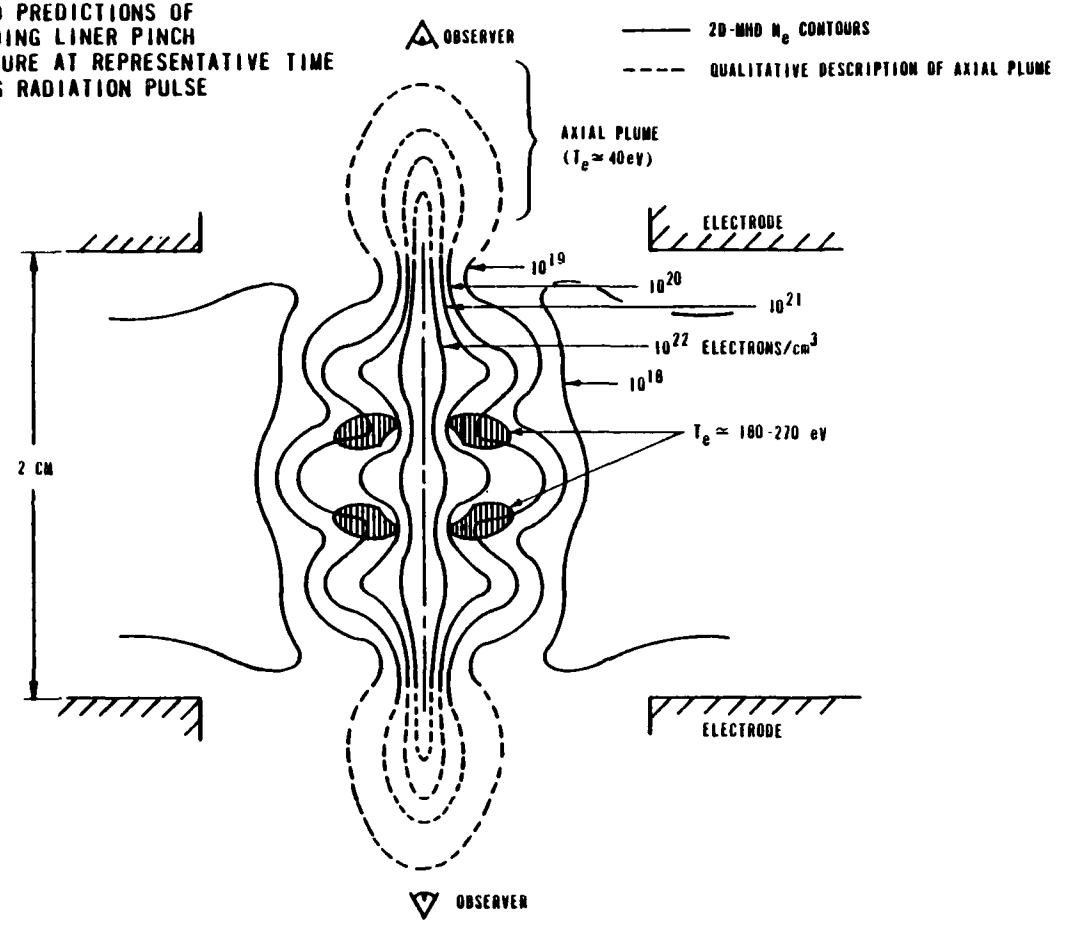

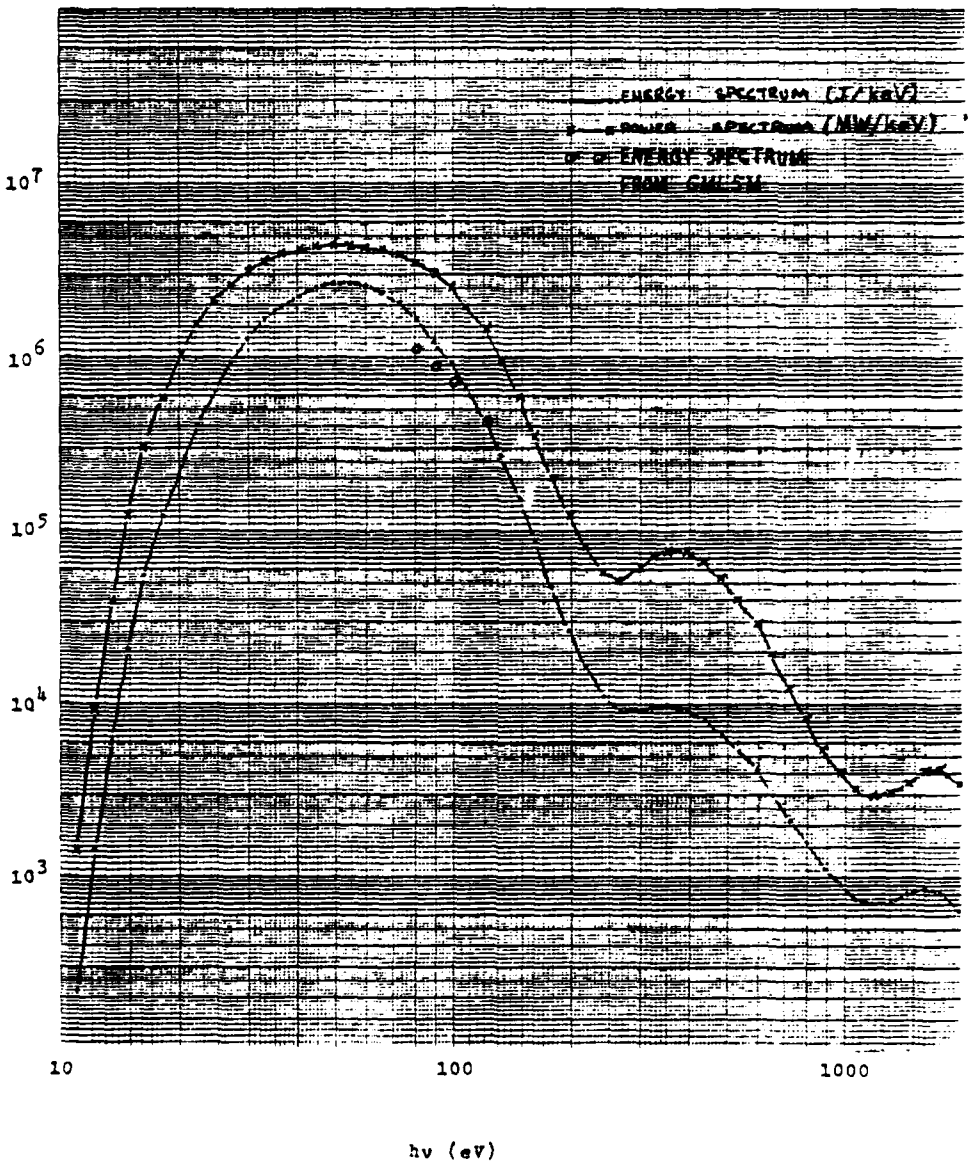

Figure IV.7. XRD Unfold Comparison

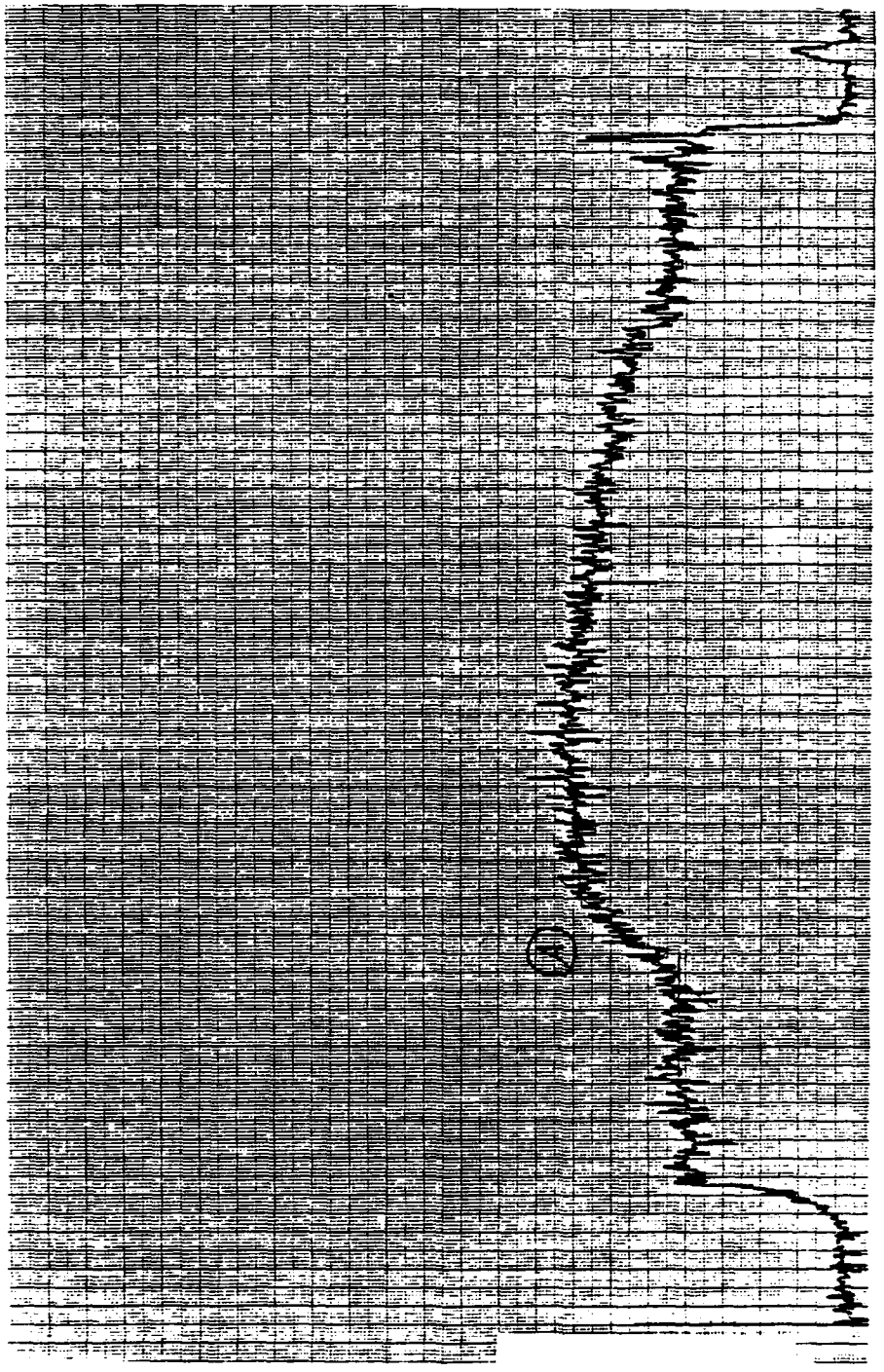

Figure IV.8. Aℓ XIII 2s-3p Line Scan

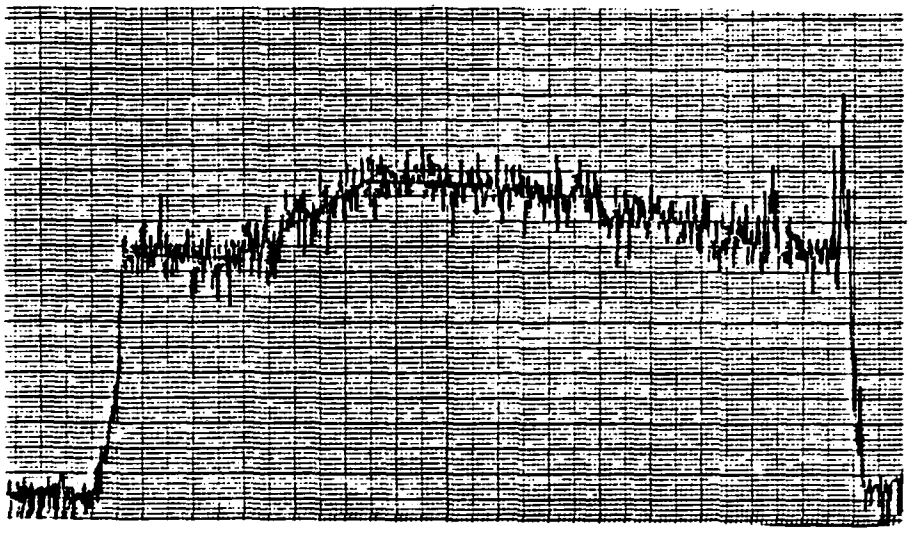

(a)

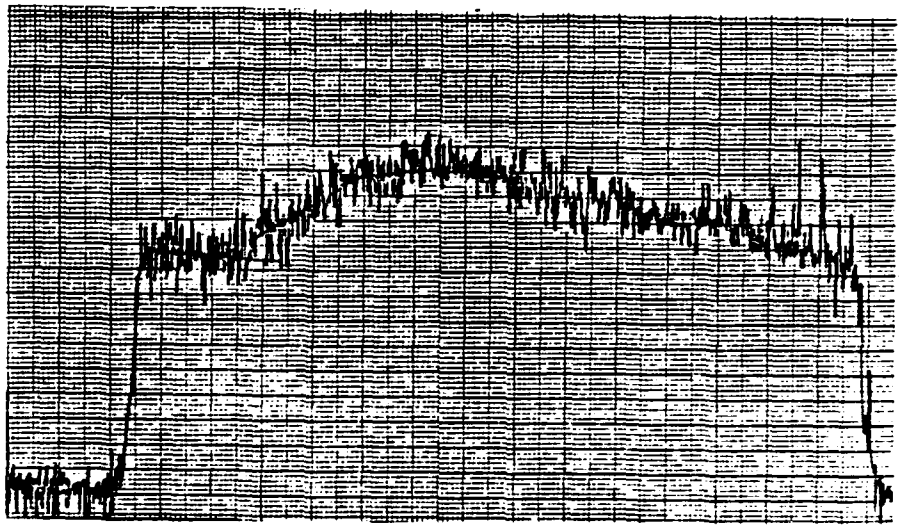

(b)

Figure IV.9. Continuum Scan

from 1.6 mm to 3.5 mm. This data is to be compared with the multicomponent plasma displayed by the 2D-MHD simulation, and is consistent with those results. It should, however, be considered tentative, awaiting further data analysis.

In conclusion, the low energy spectrum (80-580 eV) obtained by a grazing incidence spectrograph offers new insight to the spatial and spectral structure from an imploding liner experiment such as AFWL's SHIVA. The results presented here indicate the presence of a low temperature (~40 eV) axial plasma plume, filtering the emission from a hot (100-200 eV) plasma core.

V. CONCLUDING REMARKS

The interest in the experimental interaction of intense, cold REB's with dense plasmas has continued to grow, both on the computational (theoretical) side [29-34] and on the experimental side [35-36]. We expect our experimental results to have a strong impact on determining the future direction of such programatic efforts. Preliminary results, mainly diagnostic and plasma source development have been presented at a number of national technical meetings [37-38]. Details of the continued success of the SHIVA X-ray simulation program have been presented elsewhere [39-40]. Our contributions to the development and implementation of essential diagnostics has also been discussed at national meetings [41-42].

VI. REFERENCES

1. Thode, L. E. and Sudan, R. N., Phys, Fluids 18, 1552 (1975) and Phys. Fluids 18, 1564 (1975.
2. Thode, L. E., Phys. Fluids 19, 305 (1976).
3. Thode, L. E., Phys. Fluids 20, 2121 (1977).
4. Sethian, J. D. and Ekdahl, C. A, Phys. Rev. Lett. 42, 711 (1979).
5. Clark, M. C., "Foilless Diode Operation on a 7 Mev, 80 kA Electron Beam Machine," Bull. Am. Phys. Soc. 74, 1085 (1979).
6. Cheng, D. Y., Nuclear Fusion 10, 305 (1970).
7. Cheng, D. Y., "The Application of a Deflagration Gun to Fusion Systems," Proc. of High Beta Workshop, Los Alamos (1975), p. 681.
8. Clark, M. C., "Transport and Stability of a Magnetized Electron Beam Propagating Through Neutral Gas," Bull. Am. Phys. Soc. 25, 913 (1980).
9. H. R. Griem, Plasma Spectroscopy, McGraw-Hill, Inc., New York, 1964.
10. H. R. Griem, Spectral Line Broadening of Plasmas, Academic Press, New York, 1974.
11. W. L. Wiese, D. R. Pagnette, and J. E. Solarski, Phys. Rev., 129, 1225 (1963).
12. R. H. Huddlestone and S. L. Leonard, editors, Plasma Diagnostic Techniques, Academic Press, New York, 1965.
13. W. Lochte-Holtgreven, editor, Plasma Diagnostics, North-Holland Publishing Company, Amsterdam, 1968.
14. P. R. Bevington, Data Reduction and Error Analysis for the Physical Sciences, McGraw-Hill, Inc., New York, 1969.
15. See, for example, integrals 190 and 191 in Standard Mathematical Tables, 18th Student Edition, published by the Chemical Rubber Company.
16. A. Kuthy, Nucl. Inst. and Meth., 180, 7 (1981).
17. A.P.G. Kuthy, J. Appl. Phys., 50, 6139 (1979).
18. W. L. Baker et al, JAP 49, 4694 (1978).
19. The shutter design was obtained from Lockheed Palo Alto Research Labs.
20. Bank is a Magneform unit, from Maxwell Laboratories, Inc.
21. Grazing Measurements, Ltd., London, England.
22. M. G. Hobby and N. J. Peacock, J. Phys. E, Sci. Inst. 6, 854 (1973).
23. R. Speer, private communication.
24. G. F. Kiuttu, et al, Bull. Am. Phys, Soc. 24, 1057 (1979).
25. J. H. Degnan, et al, Bull. Am. Phys, Soc. 24, 1057 (1979).

26. B. Kohn, D. Kloc, and T. Hussey, private communication.
27. J. H. Degnan, et al, IEEE Int. Conf. on Plasma Sciences, Monterrey, Calif. (1978), p. 50, Conference Record.
28. P. C. Kepple and H. R. Griem, "Stark Profile Calculations for Lyman Series Lines of One Electron Ions in Dense Plasmas," NRL Memorandum Report 3634 (1978).
29. Jones, M. E. and Thode, L. E., "Theory and Simulation of Foilless Diodes," Bull. Am. Phys. Soc. 24, 977 (1979).
30. Newberger, B. S. and Thode, L. E., "Linear Theory of a Scattered Changed Particle Beam Interacting with a Collisional Plasma," Bull. Am. Phys. Soc. 24, 1097 (1979).
31. Thode, L. E., Cary, J. R., Jones, M. E., Mostrom, Newberger, B. S. and Clark, M. C., "Potential for Anomalous Generation of High Energy Density Plasma to Drive Hybrid Inertial Confinement Devices," Abstracts of IEEE Int'l Conf. on Plasma Sci, Madison, WI, 1980, p. 23.
32. Newberger, B. S., "Competition between Filamentation and Two-Stream Instabilities in a 'Cool' Relativistic Electron Beam," Bull. Am. Phys. Soc. 25, 853 (1980).
33. Jones, M. E., Mostrom, M. A. and Thode, L. E., "Analytical and Numerical Studies of Foilless Diodes," Bull. Am. Phys. Soc 25, 840 (1980).
34. Thode, L. E., Jones, M. E., Mostrom, M. A. and Morr, D. C., "Electromagnetic (Filamentation) Interaction Between a Scattered Relativistic Electron Beam and a Finite Temperature, Collisional Plasma," Bull. Am. Phys. Soc. 25, 1037 (1980).
35. Riepe, K. B., et al, "A High-Density Plasma Source Using a Current Driven Ionizing Shock Wave," Bull. Am. Phys. Soc. 25, 959 (1980).
36. Sheffield, R. L., et al., "Interaction of a Highly Collimated Intense Relativistic Electron Beam with Hydrogen," Bull. A.m. Phys. Soc. 25, 1039 (1980).
37. Len, L. K., Woodall, D. M., and Ekdahl, C. A., "Production of a High Density Plasma Target for REB Heating Experiments," Bull. Am. Phys. Soc. 25, 1011 (1980).
38. Kiuttu, G. F., Degnan, J. H. and Clark, M. C., "Stark Broadening Measurement of Relativistic Electron Beam Propagation," Bull. Am. Phys. Soc. 25, 913 (1980).

39. Baker, W. L., et al, "Neutron Production in the AFWL SHIVA Electromagnetically-driven Pinch," IEEE Int'l Conf. on Plasma Sci., Madison, WI, Conf. Abstracts IEEE 80 Ch 1544-6 NPS, p. 36 (1980).
40. Baker, W. L., et al, "SHIVA I and I' Results: Electromagnetic Implosion Generation of Pulsed High Energy Density Plasmas," High Energy X-Ray Source Technology Conf., Air Force Weapons Lab, KAFB, Albuquerque, NM, July (1980).
41. Woodall, D. M., et al, "Grazing Incidence Spectrograph Measurements of SHIVA Imploding Linear Radiation Pulse," IEEE Int'l Conf. on Plasma Sci., Madison, WI, Conf. Abstracts, IEEE 80 Ch 1544-6 NPS, p. 90.
42. Woodall, D. M., et al, "Spectral Features in the 80 eV-2 keV Energy Range from an Imploded SHIVA Foil," Bull. Am. Phys. Soc. 25, 872 (1980).


ATE
LME